Chapter-3 : Supported Metal Catalysts

Abstract

The results of studies carried out in chapter 2 were leveraged for preparing a final set of bicomponent zirconia-alumina supports by deposition-precipitation at final pH 9 using γ-Al_2O_3 as the substrate. These supports have improved microstructure. Effect of varying zirconia content is studied. N_2 physisorption is used to determine microstructure and TEM is used to understand morphology of these supports. XRD is used to study the changes in crystallite size of zirconia and interaction between zirconia and alumina in the supports. NH_3 TPD is used to study trends of acidity of the supports. Results of XRD are used to understand abrupt changes in microstructure of the supports.

Bifunctional supported metal catalysts with Co, Ni and Cu are prepared with the above supports and characterized thoroughly. The key objective is to explore the effect of zirconia content on the properties and performance of these supported metal catalysts. Of interest is also to study the influence of differences in electronic properties of Cu relative to Co and Ni on catalyst properties and performance for the transformation of styrene oxide and the hydrodeoxygenation of m-cresol.

Changes in microstructure and acidity between supports and the supported metal catalysts are compared using N_2 physisorption and NH_3 TPD respectively.

XRD is used to study changes in crystallite size and preferential orientation of crystal planes in the active metals. XPS is used for studying changes in the surface concentrations of active metals. TPR is used for studying MSI (metal support interactions) and its effect on sintering of active metals during thermal treatments, the ease of reducibility of metals and H_2 spill-over. Raman spectroscopy is also used for characterization.

The characteristics determined above are correlated with performance of these supported metal catalysts for the transformation of styrene oxide to phenylacetaldehyde and 2-phenyl ethanol (covered in chapter 4) and for the hydrodeoxygenation of m-cresol (covered in chapter 5)

3.1 Bi-component supports with varying ZrO_2:Al_2O_3 ratio

Based on outcome of studies carried out on supports in the preceding chapter (chapter 2), wherein three alumina based substrates were explored and pH of deposition-precipitation was varied over the range of 7 to 10 i.e. 7, 8, 9 and 10, at constant ZrO_2:Al_2O_3 (1 molar), γ-Al_2O_3 was selected as the substrate and pH of precipitation was set at 9 for the supports which were prepared for this part of the study. The ZrO_2: Al_2O_3 molar ratio was varied from 0 to 1. The results of the earlier study are published [1]. The basis for selection of this pH was stability of the catalyst for the decomposition of MBOH with trade-off in textural properties. The textural properties were further improved by introducing an aging step and prolonged washing to remove occluded soda.

A set of 5 supports comprising ZrO_2: Al_2O_3 with molar ratio varying from 0 to1 were prepared. The catalysts with ZrO_2: Al_2O_3 molar ratio 0.25, 0.50 or 0.75 were prepared by deposition precipitation at final pH 9. The 1:0 support was prepared by precipitation of zirconia from zirconium nitrate with aqueous soda ash. The detailed method of preparation is provided below. The 0:1 support was prepared by calcining pseudoboehmite at 550°C for 8h.

3.1.1 Preparation of bi-component zirconia alumina supports with varying Al_2O_3 and ZrO_2 ratio by deposition precipitation

The generic flow chart of final supports preparation is shown below in Figure 3.1.

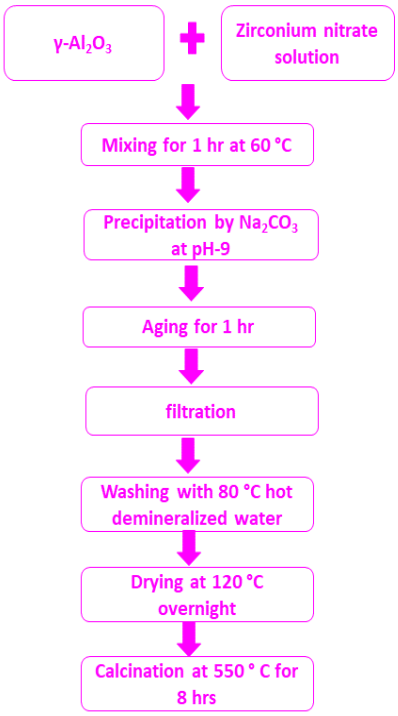

Figure 3. 1 : Schematic of method of preparation of final supports

200 g of aqueous solution of Zirconium nitrate (12.4 wt% Zr) was taken in a beaker. 184 g demineralized water and 82.2 g γ-alumina (lazer particle size 'd50' 8 μm) were added sequentially with stirring. The mixture was heated to 60°C. Zirconia was deposition-precipitated on to the γ-Al_2O_3 by adding 2.5 mol/L sodium carbonate solution (addition rate 5 ml/min) to a final stable pH of 9. The precipitate was aged in the mother liquor for 1h and then recovered by filtration. The concentration of zirconia and alumina in the filtrate were <200 ppm each, indicating near quantitative precipitation of zirconia and negligible dissolution of alumina. The precipitate was washed with hot demineralized water (80°C) to remove soda down to <500 ppm. The precipitate was dried over night at 120°C in an air oven and calcined in a flow of air in a Nabertherm make model LH 30/12 electrical furnace at 550°C for 8 h. The calcined precipitate was lightly ground to break agglomerates. The particle size was ('d50' 15 μm). The resultant solid had a nominal molar composition ZrO_2: Al_2O_3 0.25:0.75. Additional solids with ZrO_2: γ-Al_2O_3 molar ratios 0.5:0.5 and 0.75:0.25 were prepared using the method described above. Gist of preparation method and target composition of the bi-component supports is presented in Table 3.1 below.

Sr	Nomenclature	Composition	Final pH of preparation	Route of preparation
1	ZA 100	ZrO_2	9	Strike precipitation
2	ZA 75	$0.75ZrO_2$:$0.25Al_2O_3$	9	Deposition-precipitation
3	ZA 50	$0.5ZrO_2$:$0.5Al_2O_3$	9	Deposition-precipitation
4	ZA 25	$0.25ZrO_2$:$0.75Al_2O_3$	9	Deposition-precipitation
5	ZA 0	γ-Al_2O_3	-	Calcination of pseudoboehmite

Table 3. 1 : Bi-component alumina-zirconia supports with varying molar ratio

3.1.2 Materials Characterization

3.1.2.1 ICP-OES and Flame photometer

Chemical composition of the catalysts was determined by ICP-OES Thermoscientific iCAP 6000 series instrument. Argon gas was used for generating the plasma. The samples were digested in aqua regia and diluted appropriately for determining the chemical composition.

An Aimil Fotoflame Flame photometer was used to determine the sodium content of the samples.

3.1.2.2 X-ray Diffraction

This technique is non-destructive and it provides useful information such as identity of crystalline solids by fingerprinting its XRD pattern, percentage crystallinity, composition of the sample, and unit cell size. It is useful for identifying preferential orientation, changes in crystallinity etc. Inter planar distance within the solid sample is determined using the Braggs equation $n\lambda = 2d \sin\theta$, where λ is the wavelength of the X-ray radiation, d is the inter planar distance of the solid sample, and θ is the angle between the incident and diffracted radiation and n represents the order of the diffracting peak. Phase identification was done with a Bruker D8 ADVANCE X-ray diffractometer with a Cu Kα source, wavelength 1.5406 Å. Samples were

scanned in 2θ range of 5 to 80° at 2°/ min and a step size of 0.02/s. ICCD PDF4+ X-ray powder diffraction library was used for phase identification. Metal crystallite size was determined from the Scherrer equation $D = k \lambda / \beta \cos \theta$; where D is the crystal size, k is a constant, λ is the wavelength of the incident X-radiation, β is the FWHM of the diffraction peak and θ is the angle of diffraction.

3.1.2.3 N_2 physisorption:

The microstructure / texture of catalysts and catalyst supports is generally porous. It is defined by specific surface area which encompasses geometric (external surface area) and the internal surface area comprising pore walls and porosity comprising the void volume within the catalyst particle (inter particle voids). In porous solids surface area is largely internal. Pores are broadly classified by diameter as micropores (<2 nm), mesopores (2-50 nm) and macropores (>50 nm) as per IUPAC definitions. Textural properties are determined by the physisorption of nitrogen on the surface of the solid at liquid nitrogen temperatures. In general Krypton is used as the adsorbate for determining very low surface areas < 1 m^2/g. Mercury porosimetry is used for characterizing macroporous materials. The sample is evacuated at elevated temperature under vacuum and then subjected to accurate doses of nitrogen gas under vacuum until atmospheric pressure. This is followed by stepwise removal of nitrogen from the sample. The amount of gas adsorbed is determined by difference from the gas dosed and the gas which remains unadsorbed. This data is used to build an isotherm. Six types of isotherms and four types of type IV hysteresis loops are observed based on differences in texture of solids. Specific surface area of mesoporous solids is determined by the BET equation which is based on a monolayer of Nitrogen covering the surface of the catalyst. The specific pore volume is determined from the amount of nitrogen adsorbed on the sample at a defined saturation pressure. Pore size and its distribution are determined using the BJH model. This technique provides important information about the size and shape of pores which are important in catalysis from standpoint of diffusion. N_2 physisorption studies were carried out with a Quantachrome QUADRASORB SI IV. The BET specific surface area and pore volume were determined by physisorption of nitrogen at liquid nitrogen temperature. Prior to analysis, samples were degassed under vacuum at 300°C for 3 hours in a Quantachrome Make 'Flovac' degasser.

3.1.2.4 Temperature Programmed desorption

Ammonia TPD (Temperature Programmed Desorption) was carried out on a Micromeretics AutoChem-II 2920 instrument using a U shaped reactor made of quartz and a TCD detector.

For ammonia TPD, a sample of particle size 20-60 µm was pretreated in flowing helium at 550°C, followed by cooling to 50°C and saturation with ammonia (5 vol% NH_3 in Helium, 25 ml/min, 30 minutes). The sample was purged with flowing Helium gas for 60 minutes to remove un-adsorbed ammonia. The TPD was done by ramping the temperature from 50°C to 550°C at 10°C/min in a flow of pure helium.

3.2.5 Transmission electron microscopy (TEM)

TEM was carried out with a 200 kv accelerating voltage, Tecnai 20 Phillips Transmission Electron Microscope with W emitter and LaB6 electron source, S-TWIN objective lens, point resolution 0.27 nm or better, line resolution 2.0 nm or better magnification up to 75000x, CCD camera at SICART, Vallabh Vidyanagar.

3.1.3 Results and discussion

3.1.3.1 ICP-OES

The actual composition determined by ICP-OES expressed as weight % ZrO_2 and Al_2O_3 is shown in table 3.2 below. The input composition based on precursors taken for preparation is also shown in the same table.

Supports	ZrO_2 Actual (wt%)	Al2O3 Actual (wt%)	ZrO_2 Input (wt%)	Al_2O_3 Input (wt%)
ZA 100	100	0.0	100.0	-
ZA 75	78.0±0.5	22.0±0.3	78.37	21.6
ZA 50	53.5±0.5	46.5±0.3	54.7	45.3
ZA 25	29.2±0.5	70.8±0.3	28.7	71.3
ZA 0	0.0	100	-	100.0

Table 3. 2: Composition of carriers used in the study

As seen from the results, all three supports show bi-component composition close to theoretical. Na_2O was < 500 ppm in all the samples.

3.1.3.2 X-ray diffraction

XRD patterns of the five support materials calcined at 550°C 8h are shown in Figure 3.2 below. As observed from Figure 3.2, there are significant changes in the XRD pattern with variation of zirconia:γ-alumina molar ratio.

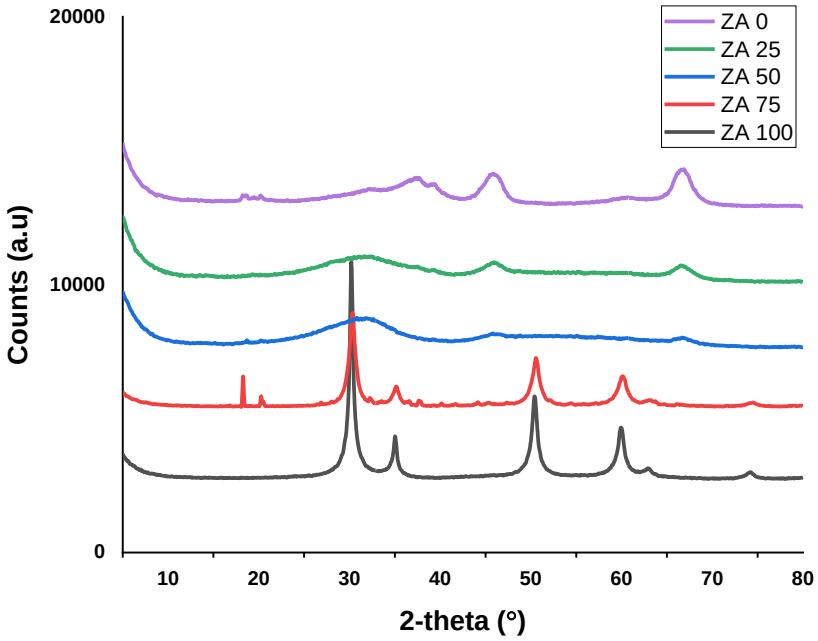

Figure 3. 2: XRD of support samples calcined at 550℃ 8h

As seen from Figure 3.2, ZA 100 (neat zirconia) and ZA 75 (75% zirconia - 25% alumina mole basis) show all 5 peaks characteristic of t-ZrO_2 (in accordance with reference PDF – 04-013-6951). Peaks of γ-Al_2O_3 are barely visible in ZA 75. The intensity of peaks of zirconia is higher in ZA 100 due to higher zirconia content and possible retardation of crystallization of zirconia by the presence of alumina in ZA 75. When the zirconia content is decreased to 50 mole% (ZA 50), the most intense peak of zirconia at 2θ 30.271° is reduced to a broad diffused peak (amorphous nature) whose maxima shifts significantly to higher 2θ. The remaining peaks of t-ZrO_2 are absent. Peaks of γ-Al_2O_3 at 2θ 45.86 and 67.034 (reference PDF-00-002-1421) are visible as very small residual peaks. The intensity of peaks of alumina are the lowest in this sample. Upon further decreasing

zirconia to 25 mole% (ZA 25) the peak at 2θ 30.271° further decreases in intensity and shifts still further to higher 2θ position. Remaining peaks of zirconia are absent. Intensity of peaks of γ-Al_2O_3 at 2θ 45.86 and 67.034 increase slightly in intensity. Support ZA 0 is of neat γ-Al_2O_3 and shows all characteristic peaks in accordance with reference PDF-00-002-1421.

The near amorphous nature of zirconia and γ-Al_2O_3 phases in calcined samples of ZA 25 and ZA 50 indicates intimate mixing/interaction between the two, such as strong interaction between the two at their interface or formation of a solid solution, which retards their crystallization at the calcination conditions used in this study. Kirsch et al.[2] have reported that when tetragonal and amorphous hydrous zirconia colloids are coated with alumina (precipitated from its propoxide) the temperature for crystallization from amorphous to tetragonal zirconia increases from 600°C to 1050°C. A similar effect is observed in the current studies when 25 or 50 mole% zirconia is deposited on the surface of γ-Al_2O_3. The crystallization of amorphous zirconia is significantly suppressed at 550°C

Morikawa et.al.[3] have proposed concept of diffusion barrier wherein alumina acts as a barrier which inhibits sintering of ceria-zirconia. Therein, they have co-precipitated ceria, zirconia and alumina to form a solid solution. Their studies show that the presence of alumina inhibits sintering of ceria zirconia. Similar inhibition of sintering is observed in the zirconia-alumina composites of the current study. Strong interaction between the two components retards crystallization of zirconia, and the composites (ZA 25 and ZA 50) tend to remain as amorphous materials upon calcination at 550°C. Since the γ-Al_2O_3 used in the study is in the form of micron sized particles (d50 8μm), temperature is 60°C and pH of preparation changes from initial acidic to 9, and the precipitate is aged for 1h in the mother liquor at these conditions, there is a possibility of local dissolution of alumina (peptization) followed by formation of zirconia-alumina solid solution.

Changes in Zr-Zr inter planar spacing d(Å) of t-ZrO_2 with decrease in zirconia content of the support is shown in Figure 3.3 below. The calculation is based on the most intense peak at 2θ 30.271° (PDF – 04-013-6951) in Figure 3.2 above.

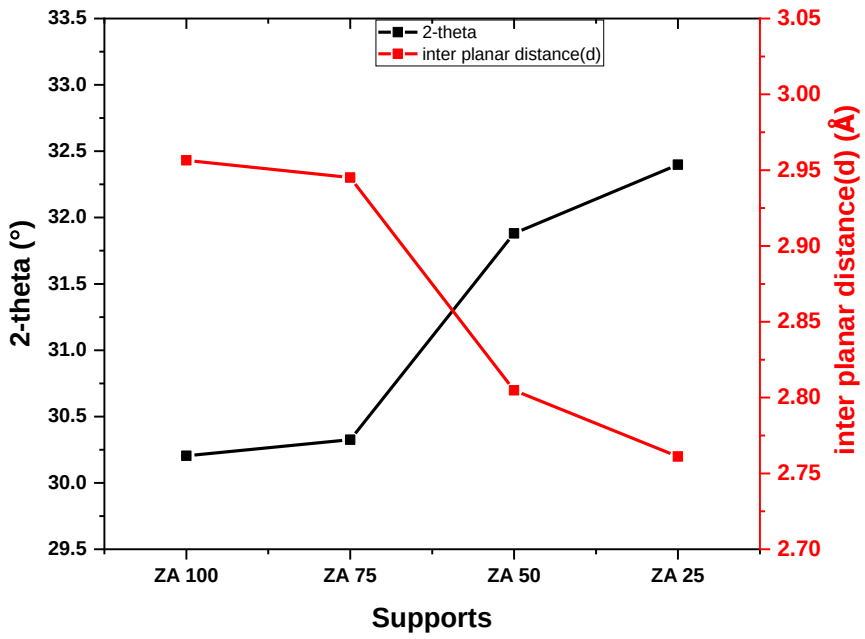

Figure 3. 3: Trend of inter planar distance of zirconia with varying zirconia:alumina molar ratio in supports

As seen from Figure 3.3 there is a clear decrease in inter planar distance of Zr from 2.94 Å to 2.76 Å (by 0.18 Å) with decrease in zirconia content. This supports incorporation of Al in the lattice of ZrO_2 like in solid solution or strong interfacial interaction between zirconia and alumina.

The crystallite sizes of ZrO_2 and Al_2O_3 determined by the Scherrer equation in the calcined support samples are presented in Table 3.3 below. Peaks at 2θ 30.271° and 67.034° for ZrO_2 and Al_2O_3 respectively are used for calculating the crystallite size.

Support	Crystallite size of ZrO_2(Å)	Crystallite size of Al_2O_3(Å)
ZA 100	180.4	-
ZA 75	105.9	BDL
ZA 50	Amorphous	62.9
ZA 25	Amorphous	43.9
ZA 0	-	43.6

Table 3. 3: Crystallite size of t-zirconia and γ-Al_2O_3 in the supports.

As seen from the Table 3.3, the crystallite size of ZrO_2 in ZA 100 and ZA 75 is 180.4 Å and 105.9 Å respectively. The decrease in crystallite size of zirconium oxide with decreasing zirconia content in the bi-component system indicates better dispersion of zirconia in bicomponent ZA 75 support. Peaks for zirconia were very broad and diffused for supports with ≤50 mol% ZrO_2 (ZA 50 and ZA 25) indicating highly dispersed zirconia on the support or its existence as an amorphous solid solution. Crystallite size of γ-Al_2O_3 is 43.6 Å in ZA 0 , it remains close to this value (43.9 Å) in ZA 25 and (62.9 Å) in ZA 50. The increase in ZA 50 could be due to strong interaction with zirconia. The peak at 2θ 67.034° is absent (BDL – below detection limit) in sample ZA 75 indicating complete dissolution of alumina in zirconia as solid solution or close interfacial interaction between zirconia and alumina which affects the XRD pattern.

3.1.3.3 BET surface area and N_2 Pore volume:

Since earlier studies which are covered in Chapter 2, with 1:1 ZrO_2:Al_2O_3 supports precipitated at pH 9 showed low surface area (about 63 m^2/g) and pore volume (0.21 ml/g), as well as presence of occluded soda, the precipitate in this case was subjected to aging followed by extended washing in this set of supports. Values of specific surface area, pore volume and average pore diameter of the supports are presented in Table 3.4 below.

Support	SSA (Specific surface area) (m^2/g)	PV (Pore volume) (ml/g)	APD (Average Pore diameter) (Å)
ZA 100	41	0.06	20
ZA 75	53	0.07	24
ZA 50	199	0.33	33
ZA 25	209	0.36	36
ZA 0	236	0.82	138

Table 3. 4: Values of specific surface area, pore volume and average pore diameter of the bicomponent zirconia-alumina supports.

As seen from Table 3.4 neat zirconia (ZA 100) shows lowest specific surface area and pore volume. Neat alumina shows highest specific surface area and pore volume. The bicomponent

supports show surface area and pore volume intermediate to that of the neat monocomponent supports. Both parameters decrease with increasing zirconia content. Average pore diameter (APD) of the bicomponent supports also decreases with increasing zirconia. However, neat zirconia has higher APD than the bicomponent supports.

From Table 3.4 it is noted that the specific surface area of samples ZA 50 and ZA 100 are significantly larger than those of supports GA-9 (65 m^2/g) and ZrO_2-9 (15 m^2/g) (Figure 2.3, chapter 2). Input composition of ZA 50 and ZA 100 is identical to that of GA-9 and ZrO_2-9 respectively. Difference in preparation method was that the ZA # supports were aged in the mother liquor after deposition precipitation, followed by extended washing. This has improved surface area significantly. Thus the aging and extended washing of the samples has paid off.

J. Angel Soto et.al.[4] have prepared alumina-zirconia mixed oxides by sol-gel method. They report specific surface area / pore volume /pore diameter 240 m^2/g / 0.46 ml/g / 51.5 Å for Al_2O_3:ZrO_2 with 25 mole% zirconia; 190 m^2/g / 0.41 ml/g / 50 Å for support with 50 mole% zirconia and 130 m^2/g / 0.35 ml/g / 44.6 Å for support with 75 mole% zirconia. Comparing their results with the results of the current study it is observed that the values are not drastically different for catalysts with zirconia content <75 mole%. Sol-gel is an expensive technique which uses organometallic compounds such as alkoxides of aluminium, such as Al tri-sec-butoxide and zirconium propoxide in the reference study. Whereas deposition precipitation is a very simple technique using economic precursors. Thus deposition precipitation is advantaged at zirconia concentrations 50 mole% and lower.

Trends of specific surface area, pore volume and average pore diameter of bicomponent ZrO_2-Al_2O_3 supports are plotted in Figure 3.4 below.

As seen from Figure 3.4, the specific surface area of these supports are in range of 235 m^2/g to 41 m^2/g. ZA-0 (neat γ-Al_2O_3) has surface area of 235 m^2/g while ZA 100 (neat ZrO_2) has surface area in range of 41 m^2/g. All other supports are having surface area in between these two values. Specific surface area decreases with increasing zirconia content. ZA-25 and ZA-50 have surface area 88 and 84% that of neat Al_2O_3 (ZA-0) whereas ZA-75 has only 22% of the surface area of ZA-100, showing a very sharp decrease when the zirconia content is increased > 50 mole%.

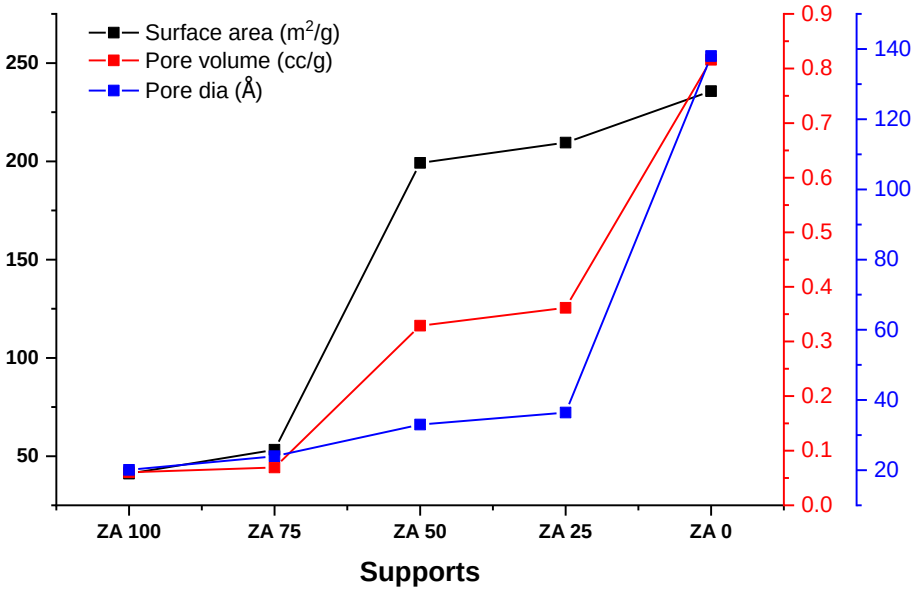

Figure 3. 4: Trends of specific surface area, pore volume and average pore diameter of bicomponent ZrO_2-Al_2O_3 supports.

Conversely, the specific surface areas of the bi-component supports are significantly higher than that of monocomponent zirconia support (ZA-100) when Al_2O_3:ZrO_2 ≥1 molar. A significant increase (jump) in specific surface area is observed relative to neat zirconia (ZA-100) upon decreasing the zirconia content below 75 mol%. The values of pore volume range decrease from 0.81 ml/g in neat alumina to 0.06 cc/g in neat zirconia. The bicomponent supports show intermediate values. They too show decrease in pore volume with increasing zirconia content in the support similar to trend of specific surface area. Similar to specific surface area, a sharp increase is observed in pore volume when zirconia content is decreased below 75 mol% in the catalysts. Thus, deposition precipitation is effective in dispersing zirconia on the substrate of γ-Al_2O_3 and thereby increasing both specific surface area and pore volume (relative to neat zirconia).

As seen from Figure 3.4 the specific surface area of ZA 0 (neat γ-Al_2O_3) decreases by 16% when 50 mole % zirconia is introduced by deposition precipitation. It then drops abruptly by ~73%

when zirconia content is further increased to 75 mole%. Likewise, the pore volume also decreases in two stages, first an abrupt decrease of ~56% when zirconia content of support is 25 mole% (ZA-25) and further decrease by 92% when the zirconia content is further increased to 75 mole% (ZA-75).

Similarly, the APD also shows abrupt decrease in two stages by ~74% at 25 mole% zirconia and further to 83% at 75 mole% zirconia.

Such trends can be attributed to plugging of the pores of γ -alumina by zirconia which is precipitated from solution. Since surface area shows only 16% drop up to 50 mole% zirconia in the support, whereas pore volume drops by 56%, it appears that relatively larger pores of the alumina substrate are partially blocked (converted to smaller pores) by the deposition of zirconia within them. When zirconia content is increased to 75 mole% there is a drastic decrease in surface area (78% cumulative) with a further loss of pore volume (up to 92% cumulative). This behavior is indicative of pore mouth plugging of the alumina substrate due to deposition of zirconia on its surface. Thus, deposition precipitation is beneficial up to 50 mole% zirconia. There is a severe loss of surface area and pore volume above this concentration. Besides other parameters, this aspect also correlates with significant decrease in activity of the transformation of styrene oxide with catalysts prepared from these supports when zirconia content is ≥ 75 mole% (Chapter 4).

The abrupt increase in specific surface area when zirconia is decreased from 75 to 50 mol% could be attributed to strong interaction / formation of solid solution of zirconia and alumina which is indeed indicated by XRD data. Results of XPS (Figure 3.19) show that the surface concentration of zirconia in support ZA 50 is 56-63% lower than expected on basis of bulk chemical analysis of this sample, which indicates shrinkage of zirconia gel. Both factors result in better availability/accessibility of alumina.

The full adsorption-desorption isotherms are shown in Figure 3.5 below.

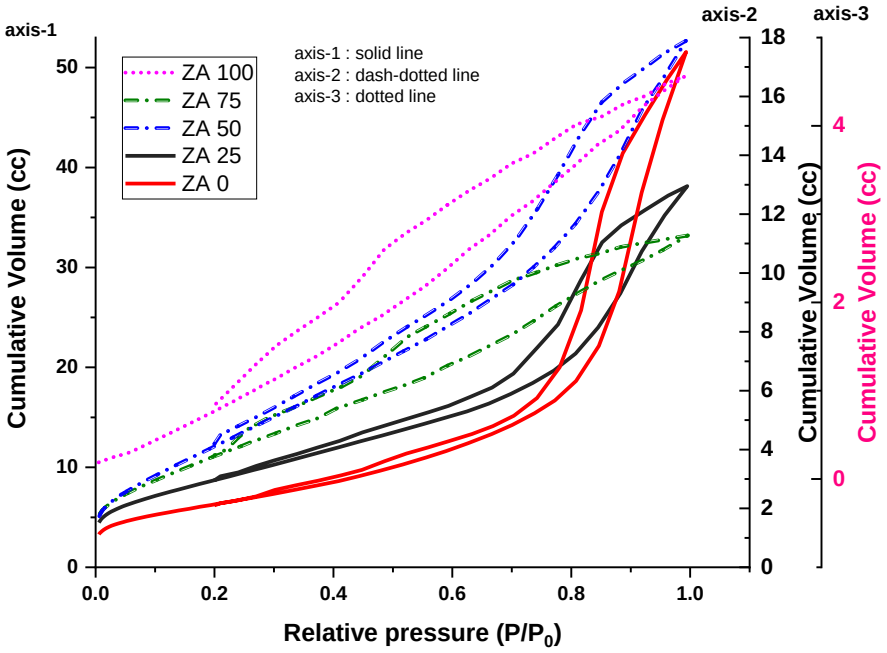

Figure 3. 5: Adsorption-desorption isotherms of the zirconia-alumina bicomponent supports: a) ZA 100, b) ZA 75, c) ZA 50, d) ZA 25 and e) ZA 0

As seen from Figure 3.5, all the isotherms are Type IV with hysteresis which is indicative of mesoporous materials. Excepting ZA-100 (neat zirconia Y axis-3) all the others show a clear 'knee' which is indicative of the point at which monolayer formation is completed[5]

The shape of the hysteresis loop is intermediate between types H1 and H4. It is clearly not H2 or H3 type, hence ink-bottle or slit shaped pores are absent. ZA 0 and ZA 25 (Y axis-1) show a clear closure of the hysteresis loop. Samples ZA 50 (Y axis-2) shows almost complete closure of the hysteresis loop whereas in samples ZA 75 (75 mole% zirconia, Y axis-2) and ZA 100 (neat zirconia) the hysteresis loop does not close completely at higher p/p0. In these latter, relatively zirconia rich samples, tendency for low pressure hysteresis is observed which is in general attributed to swelling of non-rigid porous structures, or irreversible uptake of adsorbate or severe diffusion limitation because the pore mouth approaches molecular dimensions[5]. In this specific case it appears to be due to decrease in pore mouth diameter due to deposition of zirconia.

3.1.3.4 Temperature Programmed Desorption of ammonia

Profiles of desorption of ammonia with temperature (ammonia TPD plots) of these supports are presented in Figure 3.6 below.

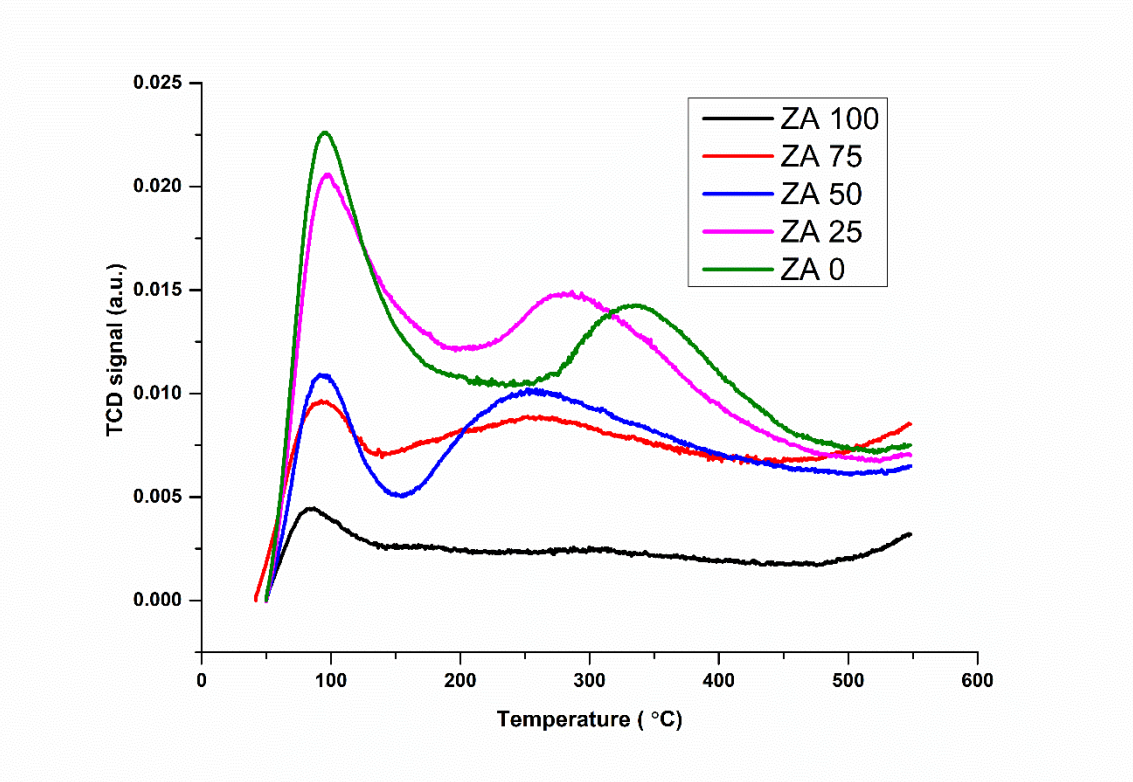

Figure 3. 6: NH_3-TPD pattern of supports used in the study.

As seen from Figure 3.6 all the supports show two peaks corresponding to weak and strong acidity. The peak area increases as the zirconia content in the catalyst decreases. The peak at about 80-100°C is due to physisorbed NH_3 (weak acidity) and the one at about 245-350°C is due to chemisorbed NH_3 (strong acidity). The latter peak is relevant to acidity responsible for reaction. ZA 100 (neat zirconia) shows barely identifiable strong acidity at about 320°C. Also seen from Figure 3.6, the maxima of the peak representing strong acidity shifts continuously to higher temperature with decreasing content of zirconia in the carrier. Thus, acid strength increases with

decreasing zirconia (increasing alumina) content of support as evidenced by shift of the peaks to high temperatures. Although ZA 75 shows significantly lower strong and total acidity than ZA 50 (Figure 3.7 or Table 3.5), its acid strength is comparable to that of ZA 50 (Figure 3.7 or Table 3.5). Large changes in acid strength are observed when zirconia content decreases below 50 mole%, such as, from peak desorption temperature 250°C in ZA 50 to 281°C in ZA 25 and 335°C in ZA 0 (γ-Al_2O_3).

Trends of weak, strong and total acidity of the supports are presented in Figure 3.7 and the values are presented in Table 3.5 below. As seen from the Table 3.5 acidity increases with increasing alumina content. Major increase (+43 mmol NH_3/g cat) in strong acidity takes place when zirconia content is decreased from 75 mole% (ZA 75) to 50 mol% (ZA 50). Further, as seen from Table 3.5, strong acidity tends to level off at 50 mol% zirconia content whereas weak acidity and total acidity level off at 25 mol% zirconia content.

The acid strength expressed as peak temperature of desorption follows a fairly linear trend (R^2 = 0.856) for strong acidity, and decreases with increasing zirconia content. Value of peak desorption at lower temperature (weak acidity) does not show any dependence on composition.

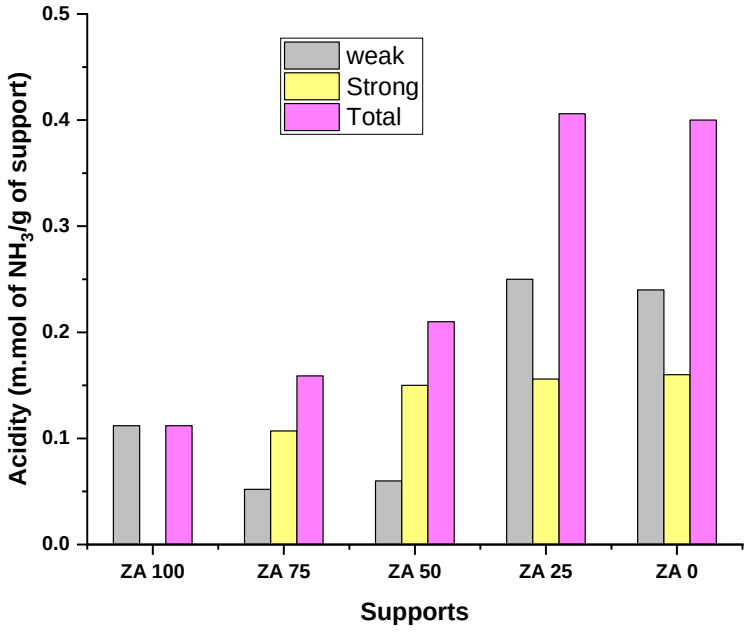

Figure 3. 7: Trend of weak, strong and total acidity of support samples.

Carrier Sample	Zirconia (mol%)	γ–Alumina (mol%)	Tmax temperature (°C)		Acidity (millimol NH_3/g carrier)		
			Low temp.	High temp.	Weak	Strong	Total
ZA 100	1	0	81	-	0.112		0.112
ZA 75	0.75	0.25	97	249	0.052	0.107	0.159
ZA 50	0.5	0.5	94	250	0.06	0.15	0.21
ZA 25	0.25	0.75	97	281	0.25	0.156	0.406
ZA 0	0	1	96	335	0.24	0.16	0.4

Table 3. 5: Values of weak, strong and total acidity and corresponding peak temperature of desorption of the supports.

As seen from Table 3.5, total moles of ammonia adsorbed per g of support increase from 112 µmol NH_3/g of support to 400 µmol NH_3/g of support as the zirconia content of the support decreases from 100% to 0% molar. Lahousse et.al.[6] have studied zirconia-alumina mixed oxides and reported that Lewis acidity increases with alumina content. Sanchez-Sanchez et.al. have also reported decrease (neutralization/moderation) of acidity of alumina when zirconia is incorporated into alumina[7]. The results of the current study are in agreement with those of Lahousse et.al. and Sanchez-Sanchez et.al. The bi-component supports show intermediate acidity between those of neat ZrO_2 (ZA 100) and neat γ-Al_2O_3 (ZA 0). Thus, it is possible to tune the total acidity of the support by changing the molar ratio of ZrO_2:Al_2O_3.

As seen from results in Table 3.5, ZA 100 shows only weak acidity. Strong acidity is practically absent in this sample (could not be integrated). The total acidity is also the lowest amongst the set of carriers. The remaining samples show both weak and strong acidity. Contribution to strong acidity is from γ-Al_2O_3.

The ratio of strong to weak acidity shows three distinct ranges with varying ZrO_2:Al_2O_3: The ratio is 0, 2.05, 2.5, 0.62 and 0.66 for ZA 100, ZA 75, ZA 50, ZA 25 and ZA 0 respectively. The ratio peaks at 50 mole% ZrO_2 in the carrier. Thus, samples containing ≥ 50 mole% ZrO_2 and those containing <50 mole% ZrO_2 in the bi-component carriers show distinct differences in this ratio.

Like textural properties discussed above, the sharp changes in strong acidity when zirconia is decreased to 50 mole% or lower is attributed to interfacial interaction or solid solution formation between zirconia and alumina, which undergoes a maximum at ~50 mole% alumina. A second possibility is shrinkage of zirconia gel during drying which increases accessibility of alumina. As seen in chapter 4, the sharp change in textural properties and acidity reflect strongly in the product distribution of transformation of styrene oxide, especially that of PAA (phenylacetaldehyde) and styrene which are favored by higher zirconia content in the carrier.

3.1.3.5 Transmission electron microscopy

Transmission Electron Microscopy of the supports was carried out to understand changes in morphology with composition.

Figure 3.8 a below shows the TEM of ZA 0 which is a neat γ-alumina support prepared by calcination of precursor pseudoboehmite at 550°C 8hr.

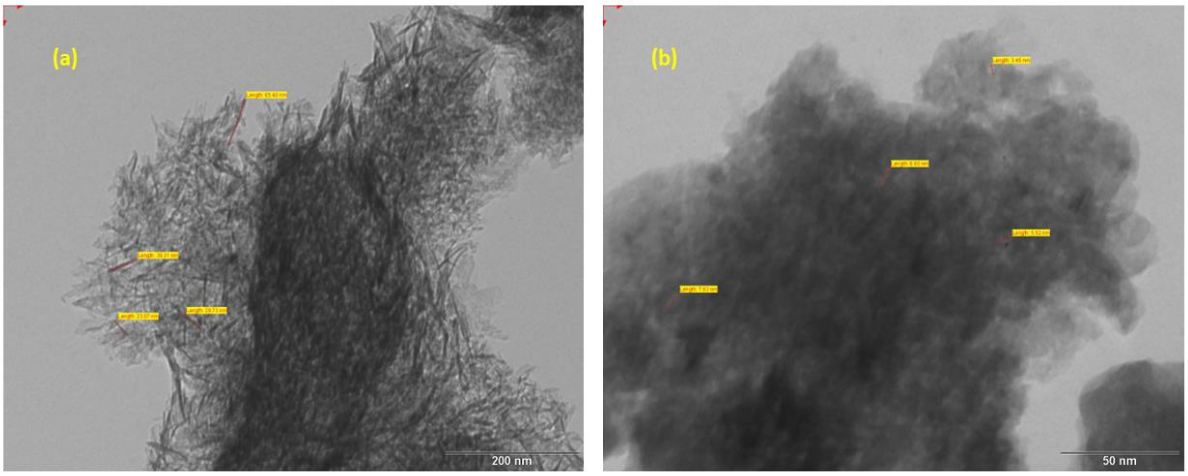

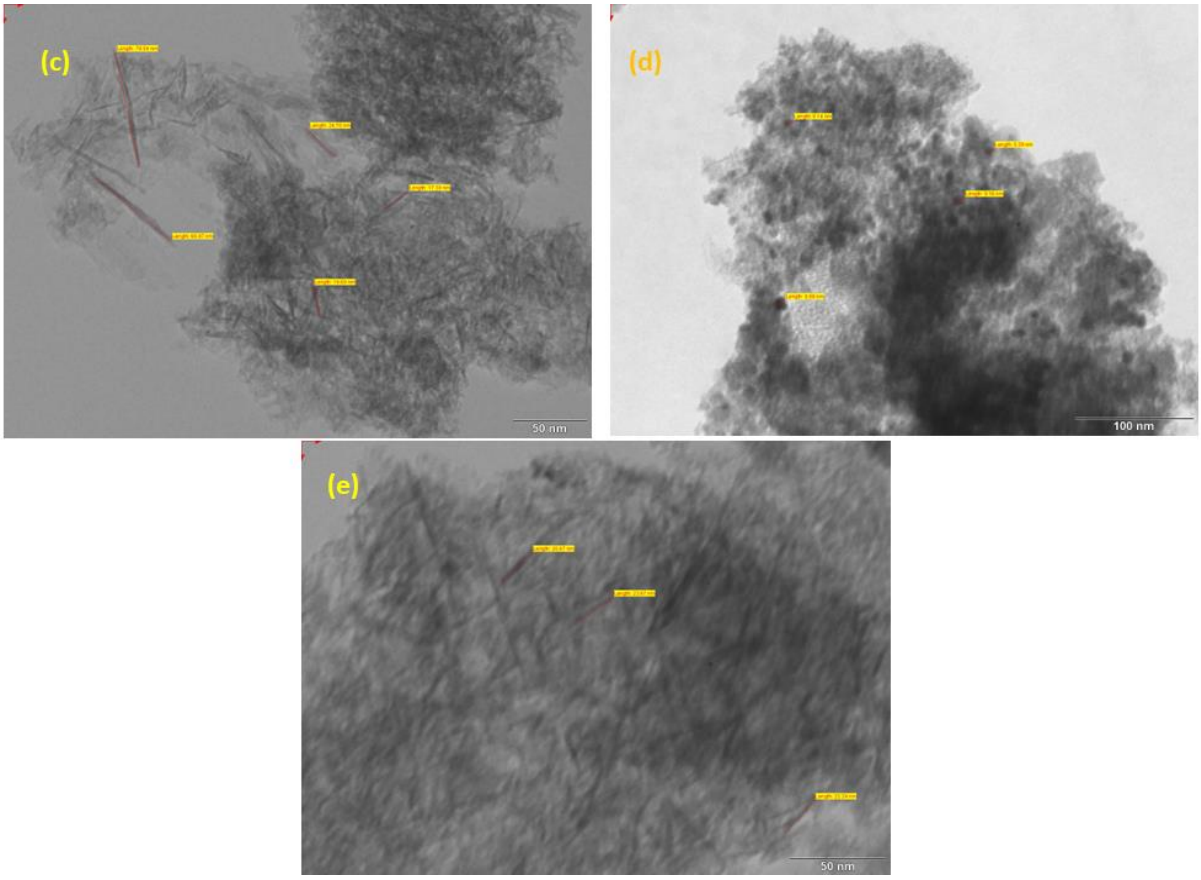

Figure 3. 8: TEM of sample of (a) neat γ-alumina, ZA-0 (b) neat zirconia, ZA 100 (c) ZA-50 (d) ZA-75 and (e) ZA-25

The micrograph shows acicular morphology, needlelike particles with length dimension 23-65 nm. The needles are intermeshed with each other forming a structure with high voids. This is typical of the parent pseudoboehmite from which the γ-Al_2O_3 was derived by calcination and explains the high surface area and pore volume of this material. Jianchuan Sun et.al. [8] have reported similar observations with respect to alumina. They report that alumina with a thin lamellar (acicular) morphology (as observed by TEM) has three times the surface area of alumina with a granular morphology.

Figure 3.8 b above shows the micrograph of ZA 100 which is neat zirconia which was prepared by strike precipitation.

Unlike ZA 0, this sample shows a dense granular morphology which is consistent with the significantly smaller specific surface area and pore volume observed by N_2 physisorption. Rounded particles with dimension 5-9 nm are observed. Dense agglomerates with much larger dimension are also evident. These particles of zirconia are seen more clearly in Figure 3.8 d (sample ZA 75). They range from micrometer to nanometer range.

The micrograph of ZA 50 which constitutes 1:1 molar zirconia:alumina is shown in Figure 3.8 c above. The sample was prepared by deposition precipitation of zirconia onto a powder of γ-Al_2O_3.

As seen from the above figure both acicular matter and dense granular phase is observed in significant amounts in this sample. The dense phase (upper right hand corner of the Figure 3.8 c) appears to be embedded in the acicular phase which leads to decreased voidage and thus decreases textural properties relative to ZA 0 or ZA 25. The rounded particles of ZrO_2 within the dense phase are in the micrometer to nanometer dimension range. Sizes of the acicular and rounded granular matter are similar to earlier micrographs.

Figure 3.8 d shows TEM of ZA 75 which contains 0.75: 0.25 molar ratio of zirconia:alumina. The sample was prepared by deposition precipitation of zirconia onto a powder of γ-Al_2O_3

As seen from Figure 3.8 d, the acicular morphology of the γ-alumina substrate is visible as embedded matter within the dense granular phase. The dense phase is the major matter as expected from the composition. The rounded particles with largest dimension 5-9 nm are attributed to tetragonal ZrO_2 which is the major component in this sample. Particles with a larger diameter (micrometer range) are also evident. Tetragonal phase of ZrO_2 was determined by XRD studies.

Figure 3.8 e shows the TEM of the ZA-25 sample which is also prepared by deposition precipitation. Its molar composition is 0.25:0.75 zirconia:alumina.

The morphology of this sample is opposite to that of ZA 75. Significant amount of acicular matter is observed along with some dense granular phase. The dense phase (ZrO_2 nanoparticles) is seen as rounded particles interspersed within the needles (of γ-Al_2O_3).

The morphology observed in TEM is consistent with the composition and it also reflects the trend of specific surface area and pore volumes of these samples. Overall both zirconia and alumina appear to be well interspersed resulting in a uniform composition at the bulk level.

Summary: In conclusion bi-component zirconia-alumina supports with varying composition were prepared by deposition precipitation. Microstructure was improved by introducing aging and extended washing to remove occluded impurities. They were compared between themselves and also with mono-component zirconia and γ-Al_2O_3 supports. Varying the composition influenced textural properties, acidity and crystallite size of zirconia. These properties can directly influence catalytic activity and product selectivity of supported metal catalysts. Abrupt changes were observed in microstructure and acidity when zirconia content in the support reached >50 mol%. The reason for this appears to be either highest interfacial interaction between zirconia-alumina / solid solution formation as indicated by results of XRD and/or better availability of γ-alumina at zirconia content $\leq$50 mol%. These supports were used for preparation of supported metal catalysts as described below.

3.2 Supported metal catalysts

The above series of supports ZA-0 to ZA-100 were used as carriers for the preparation of Co, Ni and Cu supported metal catalysts.

3.2.1 Catalyst Preparation

Supported metal catalysts were prepared by incipient wetness (dry impregnation) method. Aqueous solution of the metal nitrate equivalent in volume to the water pore volume of the carrier was heated to 65°C and added to the carrier to achieve a metal content of nominal 12 wt% (as metal) in the final catalyst. Contents were held for 30 minutes before drying at 120°C and calcining in air at 500°C, 8h. The resultant catalysts were named M-ZA ## where M stands for one of Co, Ni or Cu and ZA ## stands for the nominal mole percent of zirconia in the zirconia-alumina bi-component carrier. (refer Table 3.6 below)

Catalyst Nomenclature	Active metal	Targeted conc. of active metal (%)
Ni-ZA 100	Ni	12
Ni-ZA 75	Ni	12
Ni-ZA 50	Ni	12
Ni-ZA 25	Ni	12
Ni-ZA 0	Ni	12
Co-ZA 100	Co	12
Co-ZA 75	Co	12
Co-ZA 50	Co	12
Co-ZA 25	Co	12
Co-ZA 0	Co	12
Cu-ZA 100	Cu	12
Cu-ZA 75	Cu	12
Cu-ZA 50	Cu	12
Cu-ZA 25	Cu	12
Cu-ZA 0	Cu	12

Table 3. 6 :Series of final catalysts prepared

3.2.2 Material Characterization

All the samples were characterized by N_2 physisorption, Powder X-ray diffraction, Inductively coupled plasma analysis (ICP-OES), Temperature Programmed Desorption of ammonia (TPD), Temperature Programmed Reduction (TPR), X-ray photoelectron Spectroscopy (XPS) and Lazer Raman Spectroscopy.

3.2.2.1 ICP-OES

Chemical composition of the catalysts was determined by ICP OES Thermoscientific iCAP 6000 series. Argon gas was used for generating the plasma. The samples were digested in aqua regia and diluted appropriately for determining the chemical composition.

3.2.2.2 X-ray diffraction

Phase identification was done with a Bruker D8 ADVANCE X-ray diffractometer with a Cu Kα source, wavelength 1.5406 Å. Samples were scanned in 2θ range of 5 to 80° at 2°/ min and a step size of 0.02/s. ICCD PDF4+ X-ray powder diffraction library was used. Metal crystallite size was determined from the Scherrer equation, $D = k \lambda / \beta \cos \theta$; where D is the crystal size, k is a constant, λ is the wavelength of the incident X-radiation, β is the FWHM of the diffraction peak and θ is the angle of diffraction.

3.2.2.3 N_2 Physisorption

BET specific surface area and pore volume were determined by N_2 physisorption using a Quantachrome QUADRASORB SI IV instrument by nitrogen physisorption at liquid nitrogen temperature. Prior to analysis, samples were degassed under vacuum at 300°C for 3 hours in a Quantachrome Make 'Flovac' degasser.

3.2.2.4 Temperature Programmed Desorption:

Ammonia TPD (Temperature Programmed Desorption) was carried out on a Micromeretics AutoChem-II 2920 instrument using a U shaped reactor made of quartz and a TCD detector.

For ammonia TPD, a sample of particle size 20-60 μm was pretreated in flowing helium at 550°C, followed by cooling to 50°C and saturation with ammonia (5 vol% NH_3 in Helium, flow rate 25 ml/min, duration 30 minutes). The sample was purged with flowing Helium gas for 60

minutes to remove un-adsorbed ammonia. The TPD was done by ramping the temperature from 50°C to 550°C at 10°C/min in a flow of pure helium (flow rate 25 ml/min).

3.2.2.5 Temperature Programmed Reduction (H_2-TPR)

TPR (Temperature Programmed Reduction) were carried out on a Micromeretics AutoChem-II 2920 instrument using a U shaped reactor made of quartz and a TCD detector.

The TPR experiments were done in a similar manner as TPD by pretreating the calcined samples of the catalysts in a flow of pure Helium at 120°C for 60 minutes to remove moisture. The sample was cooled to 25°C in a flow of Helium gas. The TPR was carried out in a stream of 10 vol% H_2 in N_2 (flow rate 25 ml/min) by ramping the temperature to 800°C at 10°C/min.

3.2.2.6 X-ray Photoelectron Spectroscopy

XPS was carried out with a Scienta Omicron ESCA+ make instrument. A monochromatic Al Kα source with hν 1486.6 eV was used as X-ray source.

3.2.2.7 Raman Spectroscopy

Lazer Raman spectroscopy was carried out with a Reninshaw inVia Reflex Microscope with a Nd:YAG 532 nm lazer.

3.2.3 Results and Discussion

3.2.3.1 ICP-OES

The bulk composition of the catalysts was determined by ICP analysis. Actual bulk composition is given in Table 3.7 where the active metal contents are expressed as their oxides, (NiO, Co_3O_4 and CuO) as identified by XRD. Abbreviations and composition of the catalysts (in oxide form) are given in Table 3.7 below.

As seen from Table 3.7, average metal content across all the catalysts is 11.7 wt% and standard deviation is 1.146 for a nominal metal content of 12 wt%. The experimental values are reasonably close to the nominal value selected for preparation.

Catalyst/ Carrier Nomenclature	Metal (wt%)	Ni, Co, Cu (as oxide) (wt%)	ZrO_2 (wt%)	Al_2O_3 (wt%)
ZA 100	0.0	0.0	100	0.0
ZA 75	0.0	0.0	78.4	21.6
ZA 50	0.0	0.0	54.7	45.3
ZA 25	0.0	0.0	28.7	71.3
ZA 0	0.0	0.0	0.0	100
Ni-ZA 100	10.9	13.9	86.1	0.0
Ni-ZA 75	10.2	13.0	68.2	18.8
Ni-ZA 50	11.2	14.3	46.9	38.8
Ni-ZA 25	10.2	12.9	25.0	62.1
Ni-ZA 0	11	14.0	0.0	86.0
Co-ZA 100	10.5	14.3	85.7	0.0
Co-ZA 75	12.7	17.3	65.1	17.7
Co-ZA 50	13.0	17.7	45.2	37.1
Co-ZA 25	11.3	15.4	24.5	60.1
Co-ZA 0	10.9	14.8	0.0	85.2
Cu-ZA 100	12.4	15.5	84.5	0.0
Cu-ZA 75	13.0	16.3	65.6	18.1
Cu-ZA 50	13.0	16.3	45.8	37.9
Cu-ZA 25	13.5	16.9	23.9	59.2
Cu-ZA 0	11.9	14.9	0.0	85.1

Table 3. 7: % composition of catalysts by ICP-OES

3.2.3.2 Catalyst Microstructure:

BET specific surface area and pore volume of the catalysts are shown in Figure 3.9 below.

The trend of specific surface area and pore volume of the supported metal catalysts is similar to those of the supports, which is as expected.

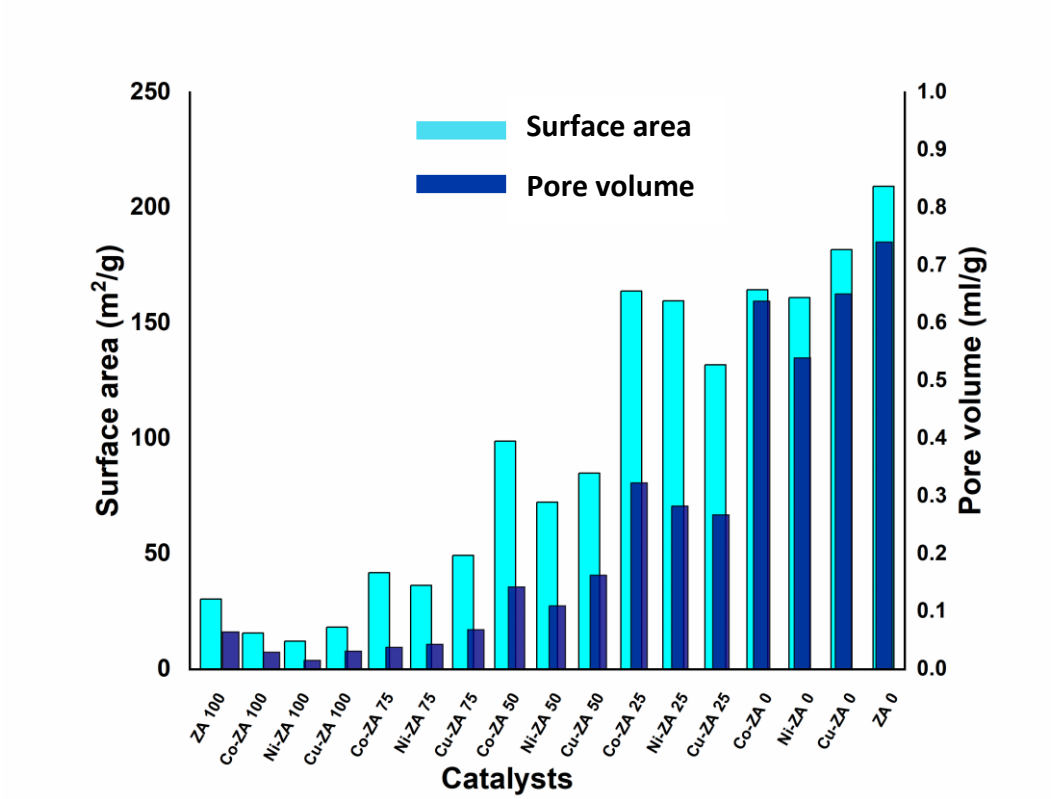

Figure 3. 9: BET specific surface area and pore volume of the catalysts determined by Nitrogen physisorption

Comparing the values of the supported metal catalysts in Figure 3.9 with those of the supports in Table 3.4, it is observed that both the specific BET surface area and pore volumes of the supports show a decrease upon incorporation of the active metals, which is typical of supported metal catalysts prepared by impregnation. The decrease in specific surface area is ~21-26% in all the M-ZA catalysts excepting for M-ZA 100 and M-ZA 50 (M= Co, Ni or Cu), where the decrease in specific surface area (relative to the support used for their preparation) is drastic, 63 and 58% average respectively. Trends of pore volume are similar to those of specific surface area. Most of the catalysts show a decrease of 10-34% whereas M-ZA 100 and M-ZA 50 show decrease of ~57% average. While the large decrease in M-ZA 100 can be attributed to the lower values of surface area and pore volume of the support ZA 100, the reason for the large decrease in the case of M-ZA 50 could not be identified.

All the Ni based catalysts show slightly lower specific surface area than their Co or Cu counterparts for a given support. Pore volume trend is also somewhat similar. The melting point

of NiO (600°C) is significantly lower than that of the other two oxides CoO (1935°C) and CuO (1326°C), which makes it more prone to thermal agglomeration. This could be a possible cause for the above observation.

3.2.3.3 X-ray Powder Diffraction:

The catalysts were subjected to powder XRD and the diffractograms are presented in Figures 3.10 a, b, c.

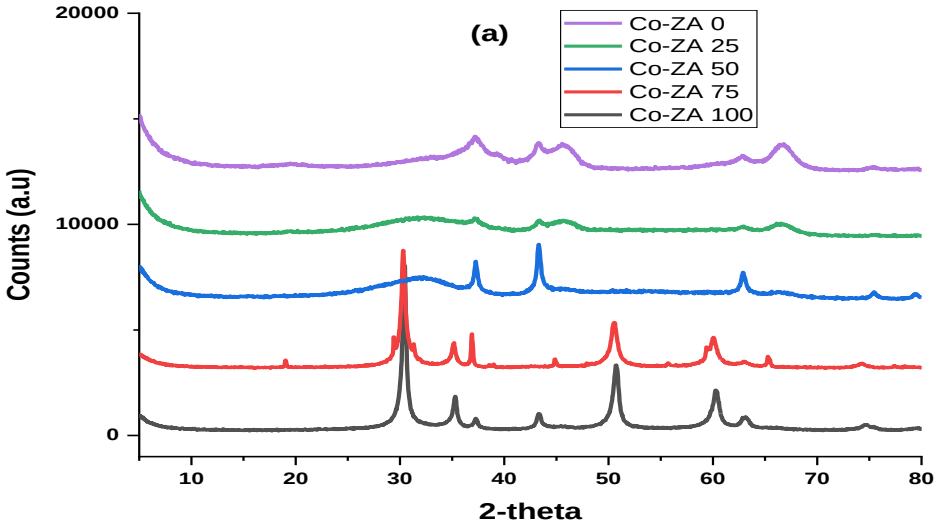

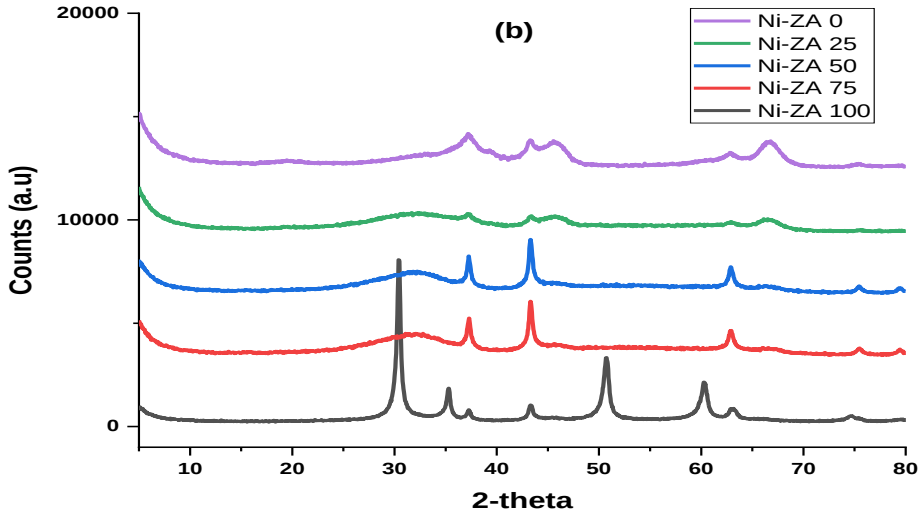

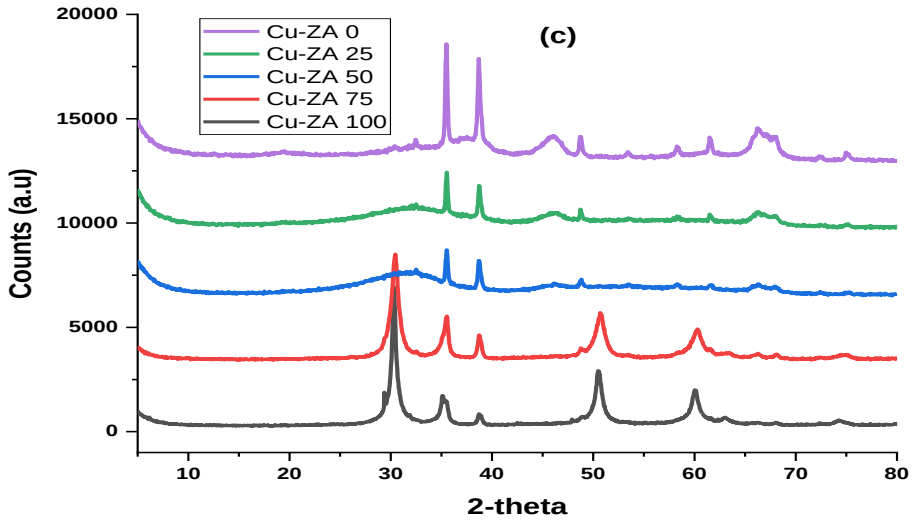

Figure 3. 10 : Diffractograms of supported metal catalysts in their calcined form. a) Co catalysts b) Ni catalysts c) Cu catalysts

Phases detected were NiO (JCPDS 04-006-1773), Co_3O_4 (04-007-2519), CuO (Tenorite 00-002-1040), ZrO_2 (Tetragonal 00-050-1089) and Aluminum oxide (gamma 00-010-0425).

Crystallite sizes of the oxides of Co, Ni and Cu determined by Scherrer equation are presented in Figure 3.11 below. The crystallite size of Cobalt oxide was determined from the d_{311} plane, that of Ni oxide from d_{200} and that of Cu oxide from d_{111}, which corresponded to the most intense peaks of these samples in the XRD diffractogram.

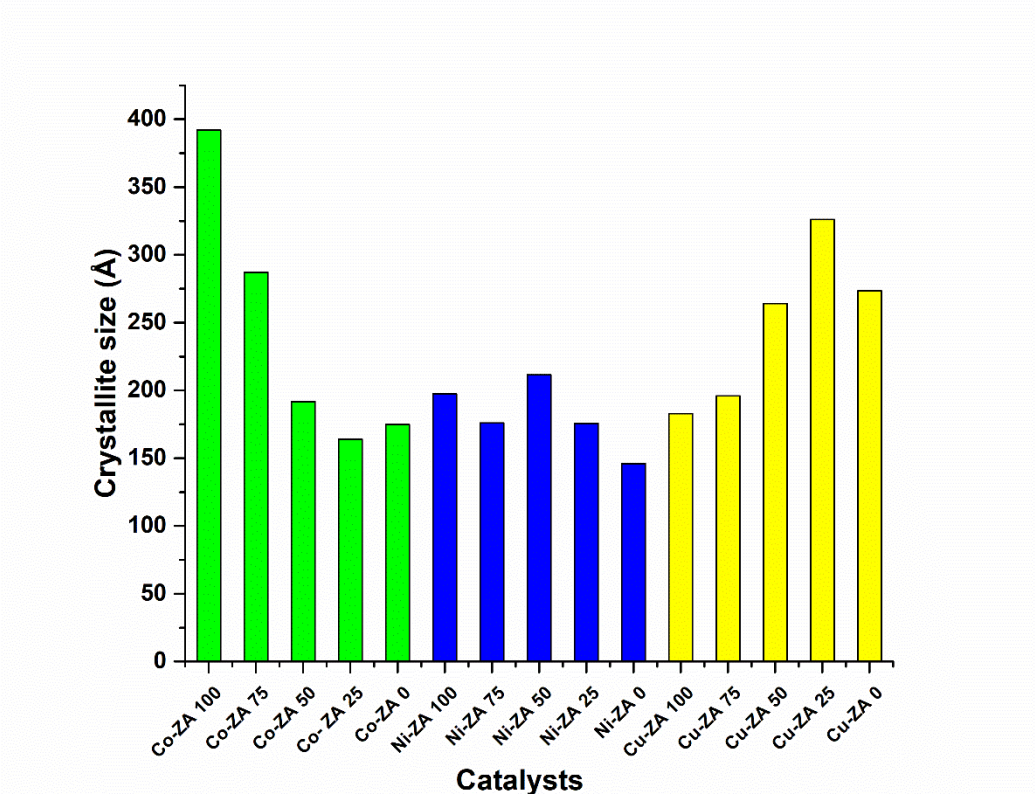

Figure 3. 11: Crystallite size of metal oxides of Co, Ni and Cu determined from powder XRD by Scherrer equation

From Figure 3.11, the crystallite size of Co_3O_4 decreases significantly (by ~54%) with decreasing zirconia content of the carrier. NiO shows a similar trend but to a smaller extent (~27%). This indicates improvement in dispersion with decreasing zirconia content of the carriers in both cases. This coincides with increasing specific BET surface area (Figure 3.4 N_2 physisorption of support/carrier) and stronger metal support interaction (MSI) of Co_3O_4 and NiO with alumina (Figure 3.14 a, b TPR).

However, CuO shows a clear opposite trend. Crystallite size of CuO is smallest when it is supported on support ZA-100 (neat zirconia) which has the lowest specific BET surface area amongst the supports (Figure 3.4). It increases by ~53% when CuO is supported on neat γ-Al_2O_3. The results of TPR (Figure 3.14 a, b, c) show that Co and Ni have stronger interaction with alumina whereas Cu has stronger interaction with zirconia. This interpretation is based on the trends of Tmax of their major reduction peak with zirconia content of the support. Thus MSI (metal support interaction) plays a key role in minimizing sintering during calcination in all three catalysts

irrespective of the active metal. Gac et.al[9] have reported similar results for Ni/Al_2O_3 and Ni/ZrO_2 catalysts. They report that Nickel is stable to sintering when supported on alumina but undergoes sintering when supported on zirconia. Since the copper catalysts supported on neat zirconia (which has the smallest surface area within the supports) shows the smallest crystallite size, it is reasoned that metal support interaction has a stronger influence on crystallite size of copper catalysts than specific BET surface area of support material.

The relative intensities of XRD peaks for Co, Ni and Cu catalysts are compared with the JCPDS reference value in Table 3.8 below.

Catalysts	XRD phase	PDF no	Miller Index	Relative intensity of hkl plane(I_r) as per PDF-4 data base	Relative intensity observed in actual analysis in M-ZA# series samples (Ir)				
			hkl		ZA-100	ZA-75	ZA-50	ZA-25	ZA-0
Co-series catalysts	Co_3O_4	04-007-2519	220	32	60	77	48	35	29
Ni-series catalysts	NiO	04-006-1773	111	64	58	57	60	79	112
Cu-series catalysts	CuO	00-002-1040	111	99	51	60	86	81	87
			110	14	0	7	38	22	8

Table 3. 8: Trend of relative intensity of XRD peaks for Co, Ni and Cu catalysts

As seen from Table 3.8 above, preferential orientation of crystal planes is observed for Co and Cu catalysts which are rich in zirconia. The (220) plane of cobalt catalysts supported on carriers with ≥50 mol% zirconia is 1.5 to 2.4 times more intense than that of the JCPDS reference relative intensity of this peak (32 units). The relative intensity of (111) plane is significantly subdued (0.5-0.6x) compared to JCPDS reference value (99 units) in the case of copper catalysts supported on carriers with ≥ 75 mol% zirconia. CuO(110) is absent in Cu-ZA 100. The corresponding reduced Cu-ZA catalysts also show the same trend for Cu(111) peak (Chapter 4 Figure 4.8). The intensity of (111) plane of Ni catalysts increases with increasing γ- Al_2O_3 content of the carrier (≥ 75 mol% alumina). But this appears to be due to contribution from the (311) plane of γ-Al_2O_3 which is a broad peak at 2-θ 37.604°, which is very close to the NiO(111) peak.

Preferred orientation of crystal planes of Co and Cu catalysts also affects intensity of peaks of Raman spectra (Figure 3.20 d, e) and influences relative selectivity of styrene in transformation of styrene oxide over these catalysts (Chapter 4, Figure 4.9 a, c).

3.2.3.4 Temperature Programmed Desorption of ammonia

NH_3 TPD profiles of Co, Ni and Cu supported catalysts are presented in Figure 3.12 a,b,c below.

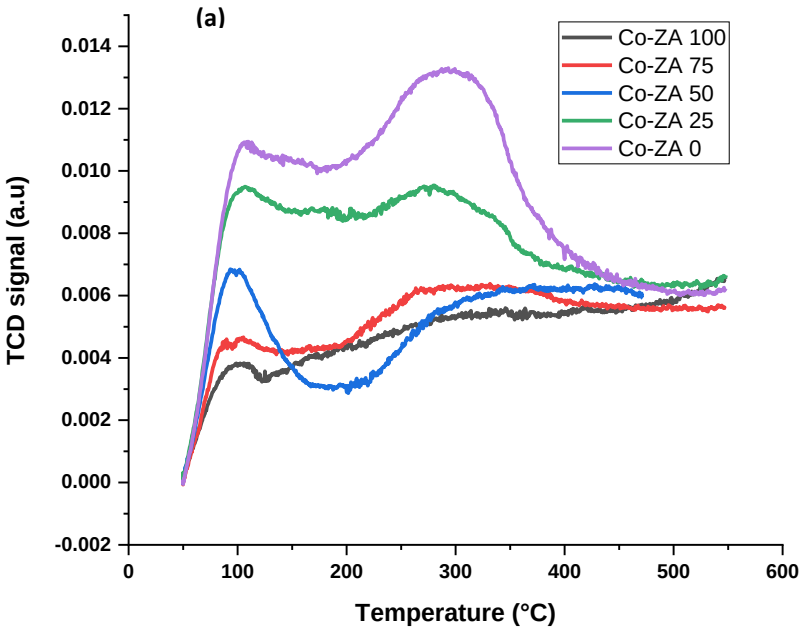

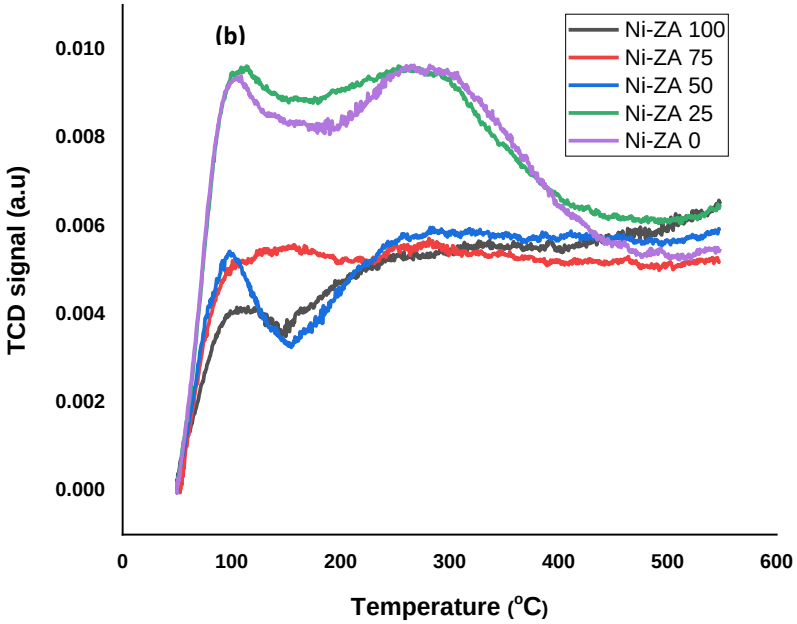

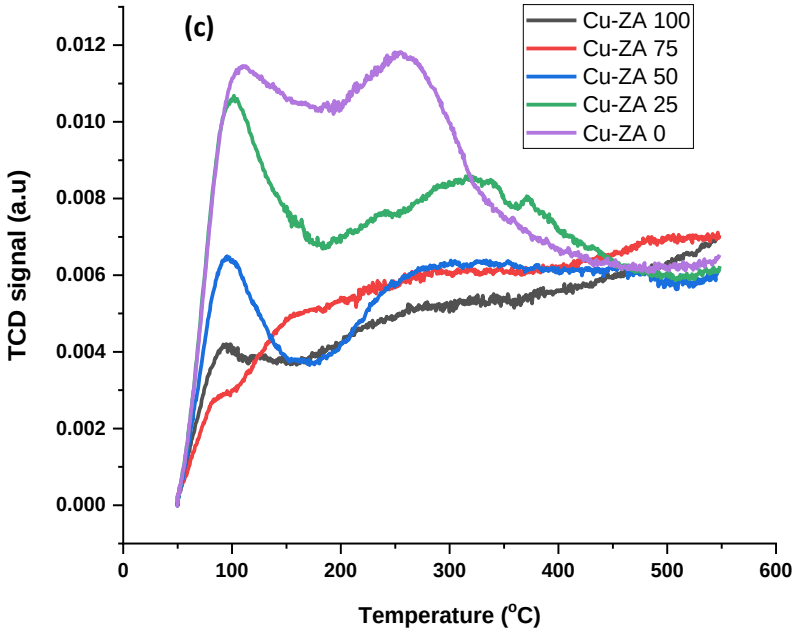

Figure 3. 12: NH_3-TPD pattern of a) supported Co catalysts b) supported Ni catalysts c) supported Cu catalysts.

As seen from Figure 3.12 a, b, c acidity increases with increasing alumina content for all the supported metal catalysts irrespective of the active metal. Acid strength also increases with alumina content of support as evidenced by shift of the peak maxima to higher temperatures.

Values of weak, strong and total acidity of supports and the three series of supported metal catalysts are presented in Figure 3.13 a, b, c, d. As seen from Figure 3.13 a, support ZA-100 (neat zirconia) does not show any strong acidity, whereas the supported metal catalysts (on ZA-100, Figures 3.13 b, c, d) show strong acidity. The source of this strong acidity is attributed to Lewis acidity arising from the oxides of the active metals supported on this carrier[10].

Comparing the acidity of the supported metal catalysts (Figure 3.13 b, c, d) with those of the supports (Figure 3.13 a) it is seen that the broad trend of acidity of the supported catalysts remains the same as that of the supports. Acidity increases with decreasing zirconia content of catalyst. However, subtle differences are observed.

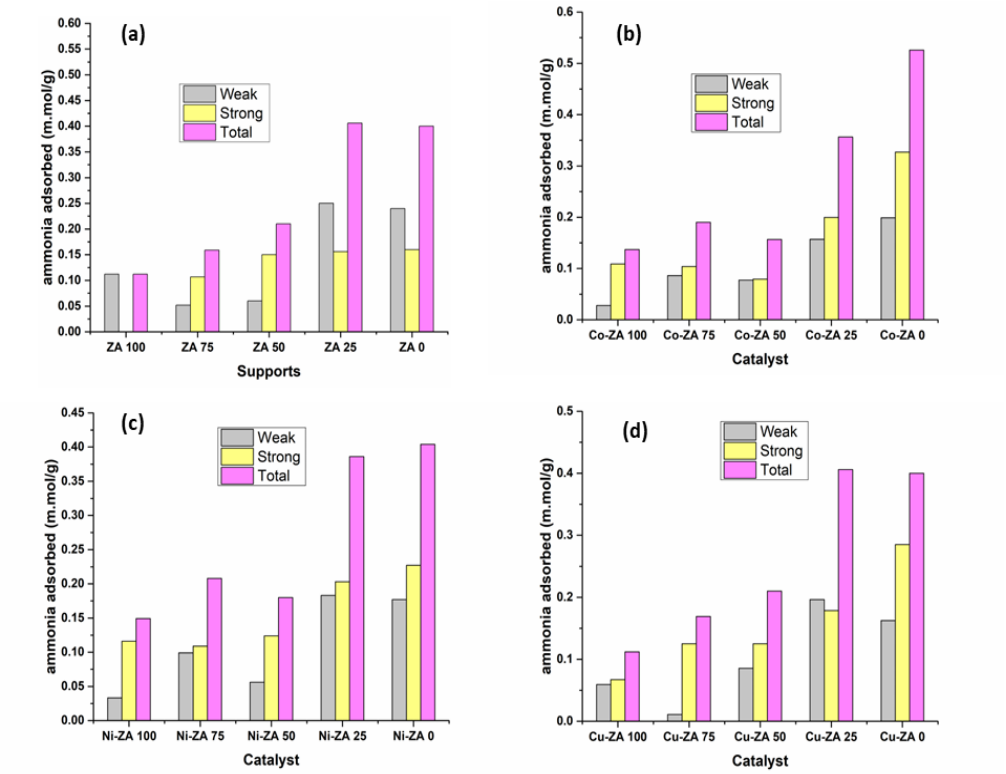

Figure 3. 13: Weak, strong and total acidity of a) carriers b) supported Co catalysts c) supported Ni catalysts d) supported Cu catalysts.

a : Trend of acidity of neat supports

b: Trends of acidity of supported Co catalysts

c: Trend of acidity of supported Ni catalysts

d: Trend of acidity of supported Cu catalysts

Once again M-ZA 50 catalysts (where M = Co, Ni or Cu) are coming as clear demarcation. Strong acidity increases in the catalysts where support is having lower than 50 mol% ZrO_2 i.e. in M-ZA 25 and M-ZA 0 metals along with alumina contributes to higher strong acidity while samples having >50 mol% ZrO_2 are showing almost similar strong acidity as their supports. Strong acidity of support ZA 50 decreases upon loading active metals. The trend is Co-ZA 50 < Ni-ZA 50 ~ Cu-ZA 50.

It is interesting to note that support ZA-100 does not present strong acidity (Figure 3.13 a) whereas the M-ZA 100 catalysts (Figure 3.13 b, c, d) present strong acidity. This is due to contribution of Lewis acidity by the active metal precursors. As seen from this figure the strong acidity of supports (Figure 3.13 a) increases with increasing alumina content till 50 mol% after which it tends to flatten out. In contrast the strong acidity of catalysts (Figure 3.13 b, c, d) increases continuously with alumina content indicating some contribution to acidity from the oxides of the active metal components. Further, the strong acidity of catalysts M-ZA 25 and M-ZA 0 significantly exceeds the strong acidity of their supports for all the three series of catalyst. Co-ZA 50 is an exception, it shows lower strong acidity than support ZA 50

Further, from Figure 3.13 b, c, d it is observed that the total quantity of ammonia adsorbed ranges from 0.126 – 0.149 mmol/g catalyst when the support is neat zirconia (ZA-100) whereas it is 3-4 times higher (ranging from 0.404 – 0.526 mmol/g catalyst) when the support is neat alumina (ZA-0).

Still further, catalysts supported on neat alumina (ZA-0) show highest acidity and higher acid strength (peak maxima in Figure 3.12).

Thus, acidity is dependent on the combination of active metal and carrier composition. These differences in acidity manifest themselves in trends of product selectivity in the transformation of styrene oxide, which is discussed in chapter 4.

3.2.3.5 Temperature Programmed Reduction

TPR profiles of Co, Ni and Cu oxides supported on the carriers with varying zirconia:alumina content are shown in Figures 3.14 a, b, c.

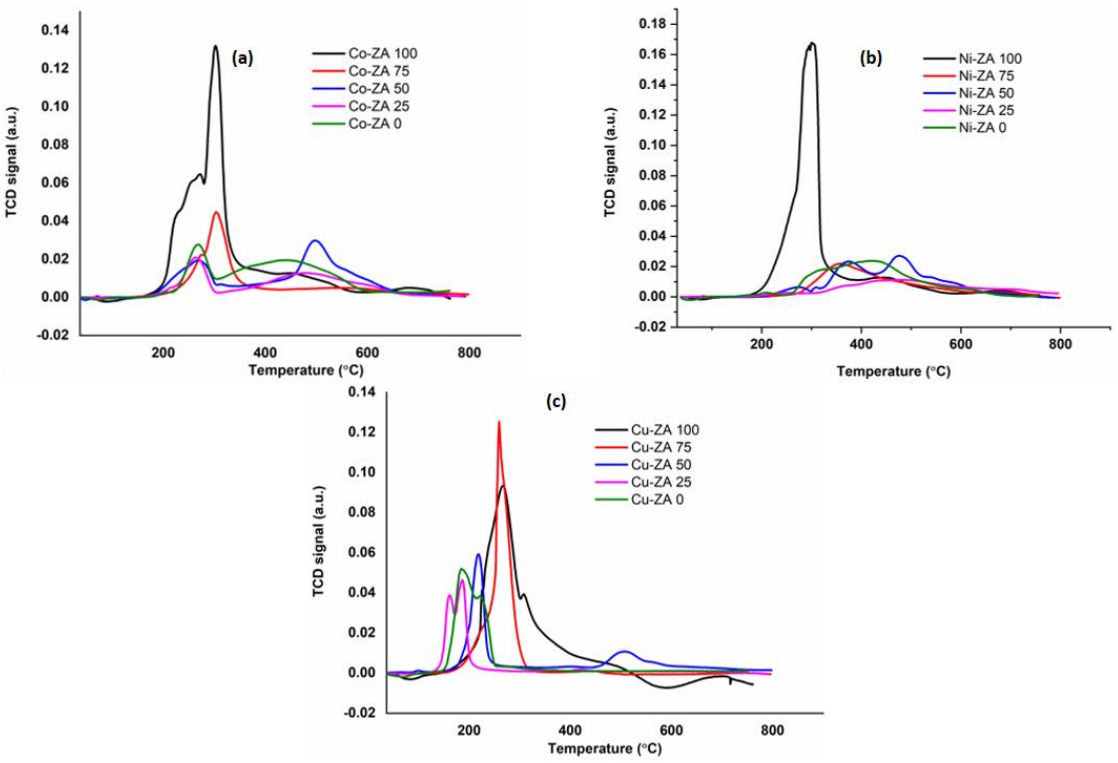

Figure 3. 14: TPR profiles of a) Co-catalysts b) Ni-catalysts and c) Cu-catalysts supported on different supports

The following distinguishing features are observed from Figure 3.14 a, b, c:

Figure 3.14 a, b and c show clear demarcation of reduction profile for the catalysts prepared with carrier containing $ZrO_2 \geq 75$ mole% and for the carriers where ZrO_2 content is < 75 mole%.

Referring Figure 3.14 a, cobalt catalysts supported on alumina rich carriers i.e. ZA 50, ZA 25 and ZA 0 show two distinct peaks, one at lower temperature around 275^{o}C and a broad second high temperature peak with maxima between 400-600°C. This indicates two types of cobalt species on alumina rich carriers or stage-wise reduction of Co_3O_4 to CoO and further to Co(0)[11] The cobalt catalysts which are prepared on zirconia rich carriers (≥75 mol%) show only one intense peak at ~300-304 °C with an ascending shoulder. This is attributed to reduction of Co_3O_4 with poor interaction with support (similar to unsupported Co_3O_4)[12]. Rajesh Munirathinam et.al.[13] have reviewed Co supported on different supports for FT synthesis. They report strong interaction between Co and alumina. They cite reference[14] which shows that the interaction between Co

and alumina decreases in zirconia modified alumina support. This is consistent with the results of the current work where the Tmax of Co supported on neat zirconia or zirconia rich carriers shifts to lower temperature and the reduction of Co on these catalysts is also completed at lower temperatures than on alumina rich supports (Figure 3.14 a)

Reduction profiles of nickel supported on bicomponent zirconia-alumina supports or on neat alumina (ZA 0) (Figure 3.14 b) are more diffuse and broad peaks range from 250°C to 600 °C, which can be attributed to reduction of nickel oxide dispersed on alumina. The high temperature peaks are attributed to Nickel having strong interaction with support. Ni-ZA 0 (neat alumina support) and Ni-ZA 25 (alumina rich support) show reduction peaks at temperature >400°C indicating strong metal support interaction. The strong interaction is attributed to incorporation of Ni into tetrahedral position in the framework of alumina[9][15]. Ni-ZA 50 shows two distinct peaks at about 390° and 490°C respectively indicating two different nickel species. Ni-ZA 75 shows a single peak ~390°C which is at lower temperature than Ni-ZA 50. Ni-ZA 100 shows a single intense peak at 300°C indicating least metal support interaction with zirconia. Wojciech Gac et.al.[9] have compared Nickel supported on alumina and zirconia. They too report stronger MSI between nickel and alumina than nickel and zirconia. In their studies nickel supported on zirconia reduces at ~300-350°C, whereas it reduces at 500°C (peak maxima) when it is supported on alumina. They also report that Ni/Al_2O_3 is more resistant to sintering. Strong MSI of Ni with alumina relative to zirconia is reported in literature which is reviewed by Lokteva et.al[15]. They also draw attention to MSI influencing reducibility and hence activity of the catalyst. The results of the current study also show reduction of Ni/ZrO_2 at about 300°C and reduction of Ni on alumina at about 400°C and 490°C which is consistent with the published literature.

The comparison between nickel and cobalt based catalysts suggests that cobalt has comparable strength of interaction with zirconia and alumina whereas nickel has stronger interaction with alumina.

Reduction behaviour of copper based catalyst is contrary to that of nickel catalysts. Most of the copper catalysts (Figure 3.14c) show bidentate peaks with their Tmax at temperature <225°C. This is attributed to stage-wise reduction of Cu(II) to Cu(I) and then to Cu(0). Copper catalysts supported on alumina rich carriers i.e. ZrO_2 < 50 mole% show lower TPR maxima than when it is

supported on zirconia rich carriers, indicating weaker metal support interaction with alumina. Sato et.al[16] have studied Cu supported on different phases of ZrO_2 for the dehydrogenation of ethanol to acetaldehyde and ethyl acetate. Their TPR studies show that Cu/t-ZrO_2 presents two reduction peaks. A major peak at 167°C with an ascending shoulder at 145°C and a minor high temperature peak at 204°C. Whereas Cu/m-ZrO_2 shows a minor peak at 145°C with ascending shoulder at 140°C and a major peak at 204°C. The TPR pattern of Cu-ZA 0 (neat zirconia support) of the present work shows a very different pattern with the major peak at about 300°C. The reason for this difference is not clear.

All three catalysts Co-ZA 50, Ni-ZA 50 and Cu-ZA 50 which are supported on carries containing 1:1 molar ZrO_2:Al_2O_3 present two well separated reduction peaks, which is different from the remaining catalysts. There appear to be two distinct types of metal-support interactions with zirconia and alumina respectively in this case. It is noted that microstructure and acidity also change abruptly when zirconia is 50 mole% in the supports. XRD studies discussed in this chapter indicate strong interaction of zirconia with alumina similar to formation of solid solution or interfacial interaction when zirconia content is 50 mole% in the support. Some residual γ-Al_2O_3 is also seen in this sample.

Ni-ZA 100, Co-ZA 100 and Cu-ZA 100 prepared with neat zirconia carrier show a single peak of high intensity which has ascending or descending shoulders. The intensity of this peak is 3 – 8 times that of the peaks of catalysts prepared using the remaining carriers. As shown in Figure 3.15 below this is attributed to spill-over of hydrogen to the support.

The ratio of the quantity of H_2 experimentally consumed in TPR and the theoretical quantity required for complete reduction of NiO, Co_3O_4 and CuO to the metal is shown in Figure 3.15 below for all the catalysts.

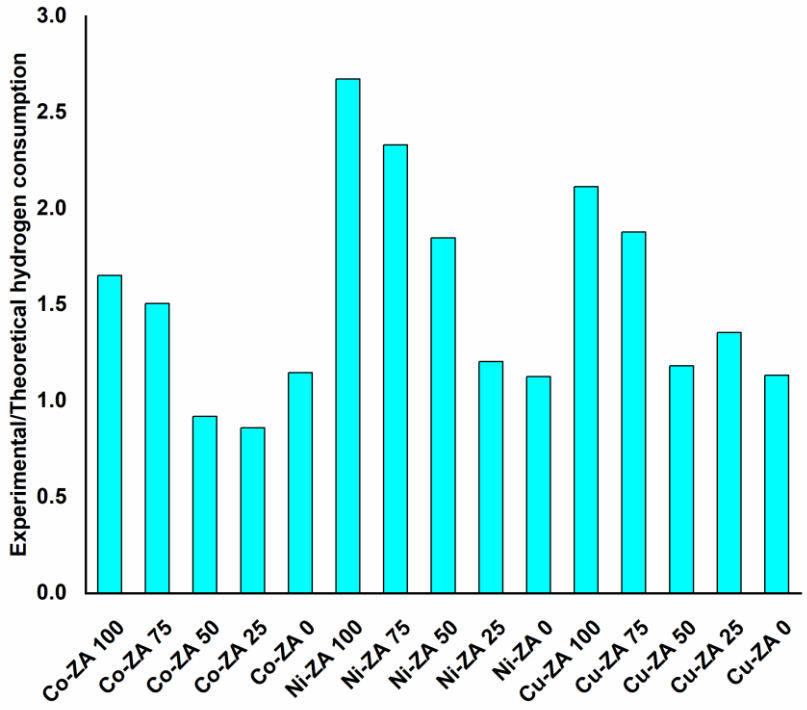

Figure 3. 15: Ratio of experimental hydrogen consumption to theoretical consumption in TPR analysis

As seen from Figure 3.15 the ratio of experimental to theoretical hydrogen consumption is significantly greater than 1 for most of the catalysts with zirconia content > 50 mol%. It tends to decrease with decreasing zirconia content of the catalyst /and approaches values closer to 1.

Pure zirconia carrier ZA 100 shows very low consumption of hydrogen, a mere 0.4 mmol/g cat compared to 2.07 - 4.96 mmol/g cat for the remaining samples. The values of H_2 uptake are not shown in Figure 3.15. The direct reduction of zirconia by hydrogen at elevated temperature is reported to be very difficult even at very severe conditions such as 2500°C[17]. Thus, the small hydrogen uptake observed in ZA 100 could be due to presence of impurity metal oxides which are reducible at the conditions of the TPR studies.

Spill-over of hydrogen from metal to zirconia is reported for Pt/ZrO_2[18] and Cu/ZrO_2[19]. Spill-over of hydrogen from Ni-Ga alloy and their intermetallic compound to SiO_2 carrier is also reported[20].

Thus, the excess hydrogen uptake observed in the current studies is attributed to spill-over of hydrogen from the metals to the carrier. As seen in chapter 4 the trend in spill-over hydrogen correlates with the selectivity for formation of styrene from SO.

3.2.3.6 X-ray Photoelectron Spectroscopy studies

The results of XPS studies of Co, Ni and Cu supported on ZA 100 (neat zirconia) and ZA 0 (neat γ- Al_2O_3) are shown in Figure 3.16 a, b, c and Figure 3.17 a, b, c below. XPS of these metals supported on carrier ZA 50 is shown in Figures 3.17 d, e and f below:

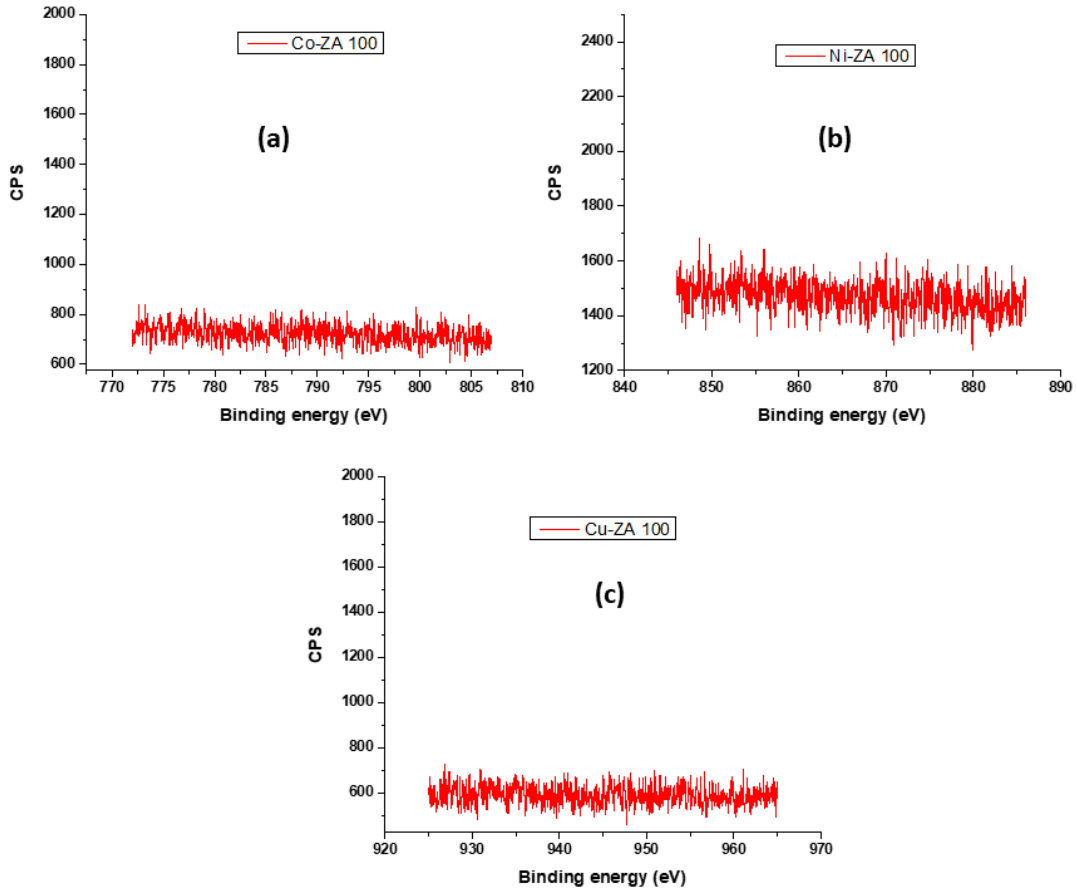

Figure 3. 16: XPS of a) Co-ZA 100, b) Ni-ZA 100 and c) Cu-ZA 100

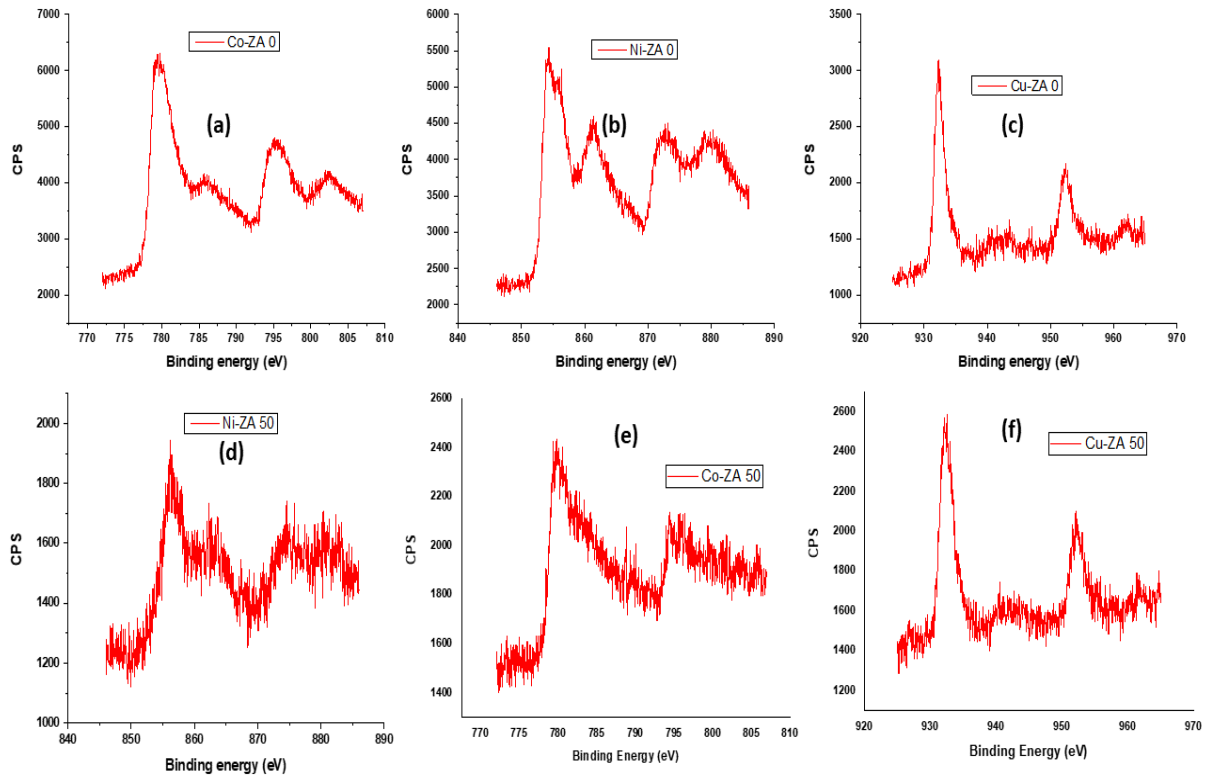

Figure 3. 17: XPS *of a) Co-ZA 0, b) Ni-ZA 0, c) Cu-ZA 0, d) Ni-ZA 50, e) Co-ZA 50 and f) Cu-ZA 50*

Comparing Figure 3.16 a, b, c with Figure 3.17 a, b, c for Co, Ni and Cu supported on neat zirconia and neat alumina respectively it is clear that:

All three active metals Ni (2p3/2 binding energy 854.32 eV), Co (2p3/2 779.37 eV), and Cu (2p3/2 932.24 eV) are clearly seen on the surface of the catalyst when the carrier is neat alumina (Figures 3.17 a, b, c respectively), whereas they are not detected (below detection limit) on the surface when the carrier is neat zirconia (Figures 3.16 a, b, c respectively).

Ni-ZA 50 (Figure 3.17 d), Co-ZA 50 and Cu-ZA 50 (Figure 3.17 e and f) which contain ZrO_2 and Al_2O_3 in 1:1 molar ratio show moderate intensity peak of the metals. Ni-ZA 50 (Figure 3.17 d) shows a peak of Ni (2p3/2 856.16 eV) with relative area which is about 25.6% of that of Ni-ZA 0. Cu-ZA 50 (Cu (2p3/2 932.24 eV) area 23.0% relative to Cu-ZA 0) and Co-ZA 50 (Co (2p3/2 779.37 eV) area 23.6% relative to Co-ZA 0) also show similar behavior.

The XPS peak area of surface concentration of active metals as a function of zirconia content of the carrier is plotted in Figure 3.18 below.

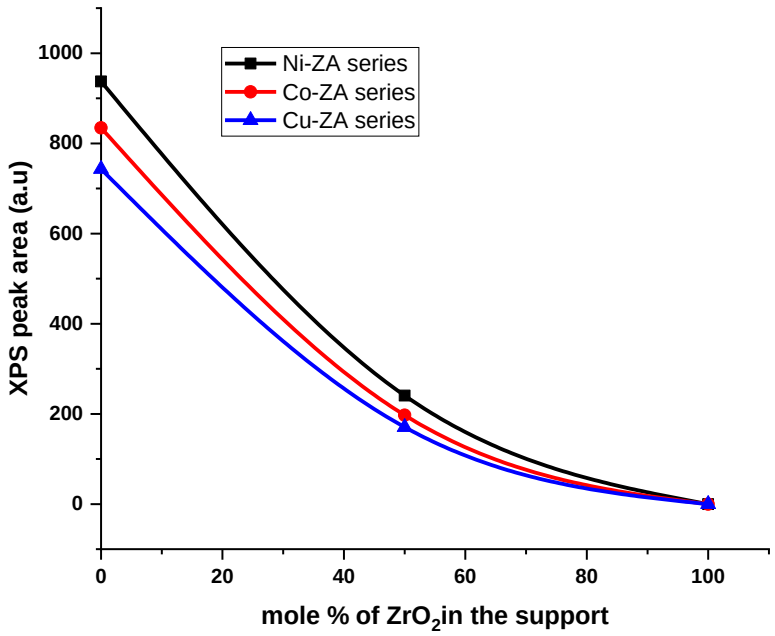

Figure 3. 18: Trend of surface concentrations of active metals in the supported metal catalysts as determined by XPS

As seen from Figure 3.18, area representing surface concentrations of all three active metals decreases sharply with increasing zirconia content and is below detection limit when the support is neat zirconia (100% zirconia). This clearly shows poor availability of active metals when zirconia content of catalyst is high. As seen in chapter 4 surface concentration of active metals affects conversion of styrene oxide and selectivity of metal catalyzed reactions (hydrogenation reactions). STY (space time yield) of 2-phenyl ethanol (2-PEA) is severely affected as a result.

ICP analysis (Table 3.7) and the other characterization techniques (XRD, TPR, Raman spectroscopy) clearly show presence of the active metals in all the catalyst samples close to target/input value. Hence, the active metals appear to migrate to subsurface layers with increasing

content of zirconia in the catalyst or agglomerate. This correlates with the low STY of 2-PEA of zirconia rich catalysts in the conversion of styrene oxide (chapter 4).

The molar ratio of ZrO_2:Al_2O_3 at the surface for catalysts supported on different bicomponent supports as determined by XPS is compared with theoretical/input values in Figure 3.19 below. Deviation from theoretical is also provided on the secondary axis of this Figure. The values of ZrO_2/Al_2O_3 (molar) and deviations are averages taken across the three series of catalysts for a given support.

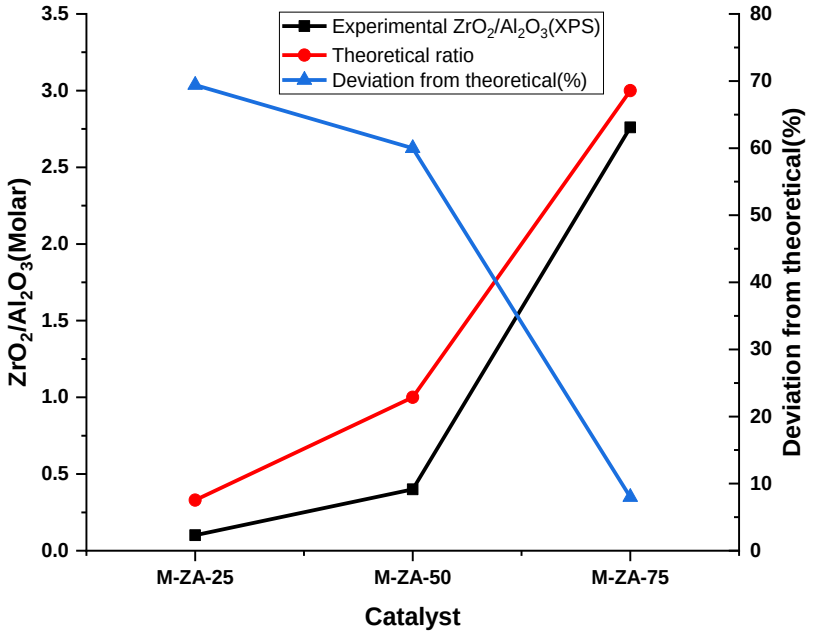

Figure 3. 19: Ratio of ZrO_2/Al_2O_3 (molar) of the supported metal catalysts as determined by XPS

As seen from Figure 3.19, the molar ratio of ZrO_2:Al_2O_3 at the surface for catalysts with ZrO2 ≤50 mol% deviates significantly from input (theoretical values). The value for M-ZA 25 is small and error can magnify. M-ZA 50 (where M = Ni or Co or Cu) deviates by 60%. ZrO_2/Al_2O_3 is 0.4 against a theoretical value of 1. Thus, surface concentration of zirconia is 60% lower than theoretical. This could be due to shrinkage of zirconia which has a gel-like texture thus resulting in significantly higher exposure of alumina. As mentioned in previous sections, surface area, pore volume and strong acidity increases substantially at ZrO_2:Al_2O_3 (1.0 molar input value). These observations also correlate with strong interaction between zirconia and alumina (solid solution

formation) as described in results of XRD. It is seen in subsequent chapters that the catalysts with mole ratio of zirconia:alumina ≤50 mole% show significantly higher catalytic activity than catalysts containing ≥75 mole% zirconia.

3.2.3.6 Raman spectroscopy

Plots of Raman spectra are shown in Figure 3.20 a, b, c, d, e below.

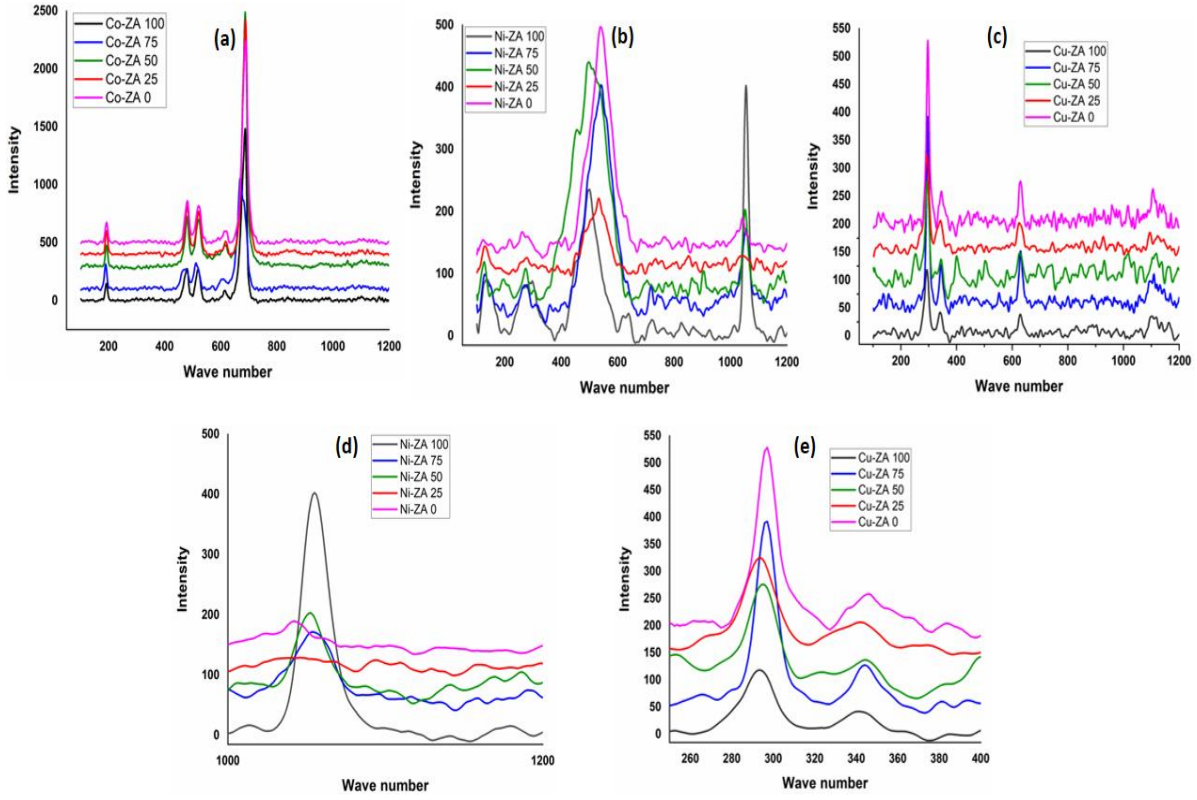

Figure 3. 20 : Raman Spectra of supported (a) Cobalt catalysts (b) Nickel catalysts and (c) Copper catalysts (d) Change in intensity of Raman band of Nickel catalysts with zirconia content (e) Change in intensity of Raman band of Copper catalysts with zirconia content

Results of Raman spectroscopy are compiled as bar charts in Figure 3.21 below. γ-Al_2O_3 is Raman inactive. t-ZrO_2 is Raman active. Raman shift bands of oxides of Co, Ni, Cu and Zr reported in literature are compiled in Table 3.9 below

Metal oxide	Symmetry	Raman shift bands (cm^{-1})	Reference
NiO	Cubic	440 (1P TO), 560 (1P LO), 730 (2TO), 930-960 (TO+LO), 1030-1080 (2LO)	N. Mironova-Ulmane et.al[21] Meza Fuentes E. et.al[22]
CuO	Monoclinic	296 (Ag), 346 (Bg), 631 (Bg)	M. Rashad et.al.[23]
Co_3O_4	Cubic	194 (F2g), 482(Eg), 522 (F2g), 618 (F2g), 691 (A1g)	M. N. Iliev[24]
ZrO_2	Tetragonal	155 (B1g), 260 (Eg), 320 (B1g), 460 (Eg), 606 (B1g), 641 (Eg)	Antonina P. Naumenko et.al.[25]

Table 3. 9: Raman transitions of pure metal oxides

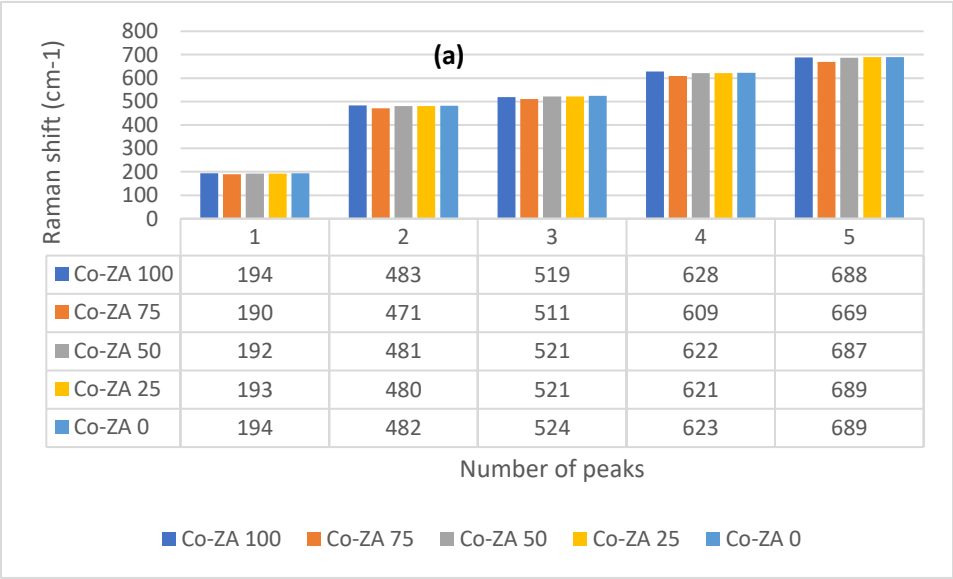

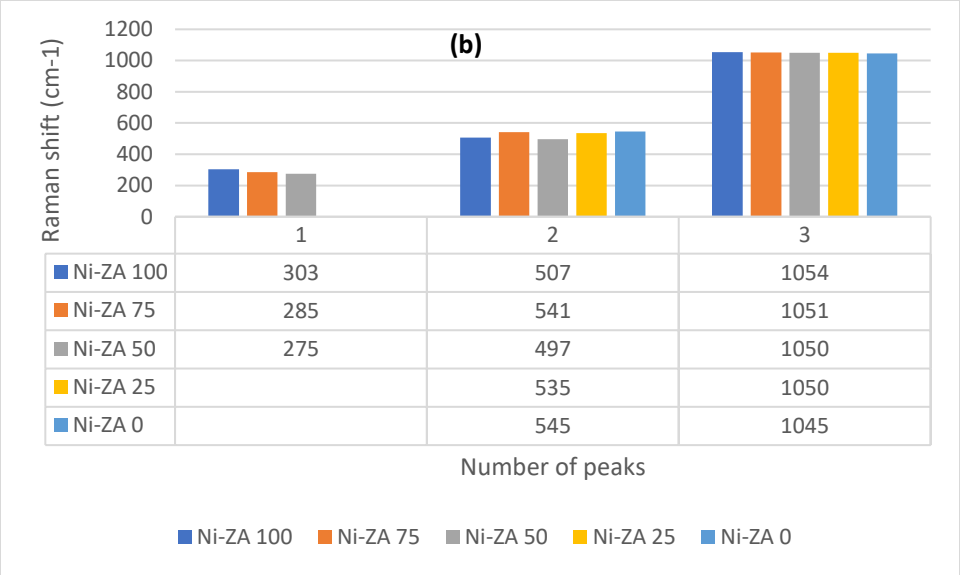

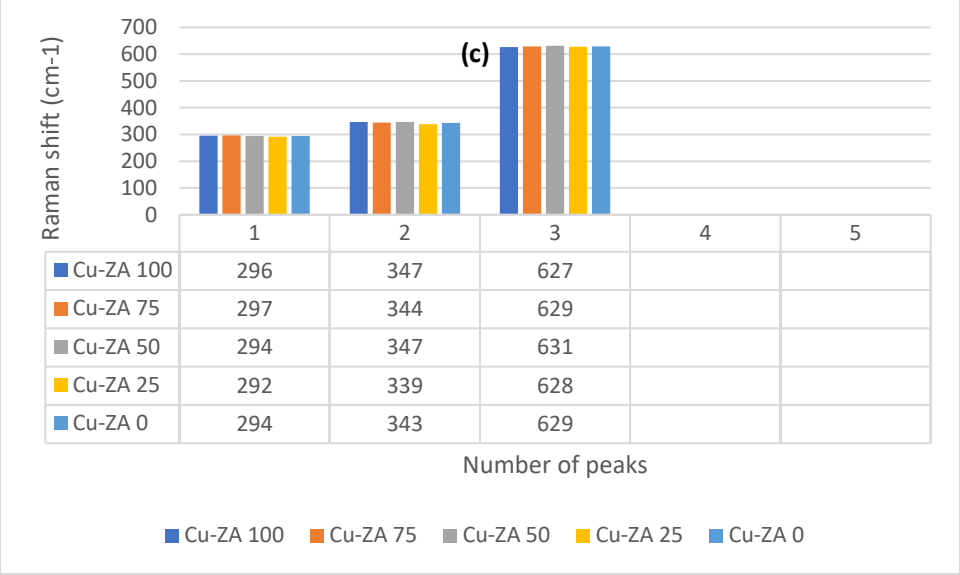

Figure 3. 21: Raman shift bands of a) Co catalysts, b) Ni catalysts c) Cu catalysts supported on zirconia-alumina

The following trends are observed by comparing the transitions in Figure 3.21a-c with the Raman transitions listed in Table 3.9:

Referring Figure 3.21a): The supported Co catalysts exhibit all five Raman transitions characteristic of Co_3O_4 spinel[23]. The peak in the 522 cm^{-1} region shows a Blue shift of 5 cm^{-1}

(from 519 to 524 cm^{-1}) when the support changes from neat zirconia to neat alumina, indicating strengthening of the Co-O bond.

Referring to Figure 3.21b): All the Nickel catalysts show two transitions one each of 1P LO (497-541 cm^{-1}) and 2P LO (1045-1055 cm^{-1}). The intensity of the latter band decreases with increasing alumina content (Figure 3.20 d). Decrease or disappearance of this band is reported for NiO[21], NiO/Al_2O_3[26] and for Ni-Al hydrotalcites[22]. The decrease in intensity is attributed to a decrease in crystallite size, metal support interaction or decrease in particle size of NiO respectively. This corroborates with results of XRD which show decrease in crystallite size with increasing alumina in the catalyst. All the Ni catalyst samples show two additional transitions at (275-303 cm^{-1}) and (130-140 cm^{-1}) which are relatively more prominent for samples containing zirconia. These are attributed to tetragonal zirconia. The peak in the 540 cm^{-1} region shows a strong Blue shift of 38 cm^{-1} (507 to 545 cm^{-1}) when the support changes from neat zirconia to neat alumina, indicating strengthening of the Ni-O bond, similar to Co catalysts. TPR too shows stronger MSI of Ni with alumina. Referring to Figure 3.21c): All the supported Cu catalysts show all three Raman bands characteristic of CuO (Tenorite). Samples with >50 mol% zirconia show significantly higher intensity of the band at about 295 cm^{-1} than the remaining samples of Cu based catalysts (Figure 3.21 e). This correlates with XRD studies which show low relative intensity of the 111 plane of CuO. Preferential orientation of Cu(200/graphene and its effect for oxidation, reduction and coupling reactions is also reported in literature[27]. Contrary to the Co and Ni catalysts, a weak red shift of 2 cm^{-1} (296 to 294 cm^{-1}) is observed for the band at 296 cm^{-1}, indicating weakening of the Cu-O bond as support changes from neat zirconia to neat alumina. TPR indicates weaker metal support interaction between CuO and Al_2O_3.

These supported metal catalysts were evaluated for their activity in transformation of styrene oxide and for the hydrodeoxygenation of m-cresol, results of which are covered in chapters 4 and 5 respectively. Performance trends were correlated with characteristics of the catalyst to identify structure-activity correlations.

3.2.4 Conclusions

Thus, it is observed that:

1. Deposition precipitation results in uniform bulk distribution of zirconia within a matrix of γ-Al_2O_3. The zirconia is present in the form of rounded particles which are 5-9 nm in size. Agglomerates of micrometer size are also observed. Alumina shows an acicular morphology. Bulk composition of the bicomponent supports is close to target/input values.
2. Zirconia appears to be well dispersed within the alumina matrix when its molar concentration in the bicomponent support is ≤50 mole%. Zirconia is not detected by XRD in these cases. This is indicative of strong interaction between zirconia and alumina which could be interfacial or even formation of solid solution
3. The high specific surface area and pore volume of γ-Al_2O_3 (ZA-0) are due to intermeshing of acicular particles resulting in open voids (results of TEM). Significantly lower values in neat zirconia ZA-100 are due to presence of dense granular phase which shrinks during drying. Thorough washing of the precipitate removes occluded sodium and also increases surface area and pore volume. Shrinkage of zirconia has a profound influence on textural properties and acidity.
4. Results of XPS, specific surface area, pore volume, acidity and conversion of styrene oxide indicate that there is a significant change in the character of the support ZA 50 which could be due to strong interaction between zirconia and alumina / formation of solid solution. This reflects in higher than expected surface concentrations of γ-Al_2O_3 when the zirconia content is ≤50 mole% in the catalysts (XPS). This corroborates with sharp increase in the surface area, pore volume, acidity and activity for these samples (conversion of styrene oxide which is presented in chapter 4). The changes in surface concentration of active metals influences activity (conversion of styrene oxide) as presented in chapter 4.
5. Influence of zirconia: Increasing mole ratio of ZrO_2:γ-Al_2O_3 in the bicomponent supports decreases acidity and acid strength. It also decreases surface concentration of active metals. Significant changes in these parameters are observed when the concentration of ZrO_2 in the support is decreased to 50 mole% or lower. Changes in acidity and surface concentration of active metals strongly influence selectivity of phenylacetaldehyde in the transformation of styrene oxide (which is presented in chapter 4) and product selectivity between TAU (Tautomerization) and HDO (hydrodeoxygenation) in the hydrodeoxygenation of m-cresol (Chapter 5)

6. Certain combinations of metal and acid function have a strong influence on product selectivity in the HDO (hydrodeoxygenation) of m-cresol (as presented in Chapter 5)
7. Zirconia also influences preferential orientation of (111) plane of CuO in supported copper catalysts and the (220) plane of Co_2O_3 in supported cobalt catalysts. The former is strongly subdued while the latter is enhanced when zirconia content is ≥75 mole%. This trend also reflects in reduced catalysts. This appears to contribute to the significantly higher selectivity to styrene at expense of 2-PEA in the transformation of styrene oxide (which is presented in chapter 4)
8. TPR clearly shows that CuO has a strong interaction (MSI – metal support interaction) with zirconia, whereas Co_2O_3 and NiO have stronger interactions with γ-Al_2O_3. This reflects in the trend of crystallite size determined by XRD. Zirconia also influences H_2 spillover to support. Higher zirconia content results in higher spillover.
9. Influence of MSI on crystallite size is also seen in spent catalysts which are reduced at 450°C. (Covered in Chapter 5, Figure 5.3). Copper catalysts with high alumina content show sintering during reduction due to low metal support interaction. Cobalt catalysts do not show a significant change. Nickel catalysts supported on zirconia rich carriers show sintering/agglomeration whereas those supported on alumina rich carriers show redispersion (increase in metal surface area).
10. Raman spectroscopy shows changes in intensity of peaks which is indicative of changes in dispersion, metal support interactions or preferential orientation of XRD planes.

Thus, varying zirconia:alumina changes a host of properties which in turn influence trends of activity and product selectivity in transformation of styrene (Chapter 4) and hydrodeoxygenation of m-cresol (Chapter 5). Copper catalysts show different characteristics than their Co and Ni counterparts. Copper is also known to have electronic properties which are different from those of Co or Ni, which could be responsible for difference in characteristics and behavior.

3.2.5 References

[1] R. H. Pathan, C. K. Modi, and A. Basrur, “Effect of pH on the detailed chemical nature and metal-carbonate species in as synthesized zirconia alumina composites,” *J. Am. Ceram.*

Soc., vol. 103, no. 11, pp. 6615–6629, Nov. 2020, doi: 10.1111/jace.17368.

[2] B. L. Kirsch and S. H. Tolbert, "Stabilization of Isolated Hydrous Amorphous and Tetragonal Zirconia Nanoparticles Through the Formation of a Passivating Alumina Shell," *Adv. Funct. Mater.*, vol. 13, no. 4, pp. 281–288, 2003, doi: http://dx.doi.org/10.1002/adfm.200304267.

[3] A. Morikawa, T. Suzuki, T. Kanazawa, K. Kikuta, A. Suda, and H. Shinjo, "A new concept in high performance ceria–zirconia oxygen storage capacity material with Al2O3 as a diffusion barrier," *Appl. Catal. B Environ.*, vol. 78, no. 3, pp. 210–221, 2008, doi: http://dx.doi.org/10.1016/j.apcatb.2007.09.013.

[4] J. Ángel-Soto, M. Martínez-Rosales, P. Ángel-Soto, and A. Zamorategui-Molina, "Synthesis, characterization and catalytic application of Ni catalysts supported on alumina–zirconia mixed oxides," *Bull. Mater. Sci.*, vol. 40, no. 7, pp. 1309–1318, Dec. 2017, doi: 10.1007/s12034-017-1493-y.

[5] K. S. W. Sing, "Reporting physisorption data for gas/solid systems with special reference to the determination of surface area and porosity (Provisional)," *Pure Appl. Chem.*, vol. 54, no. 11, pp. 2201–2218, Jan. 1982, doi: 10.1351/pac198254112201.

[6] C. Lahousse, A. Aboulayt, F. Maugé, J. Bachelier, and J. C. Lavalley, "Acidic and basic properties of zirconia—alumina and zirconia—titania mixed oxides," *J. Mol. Catal.*, vol. 84, no. 3, pp. 283–297, Oct. 1993, doi: 10.1016/0304-5102(93)85061-W.

[7] M. SANCHEZSANCHEZ, R. NAVARRO, and J. FIERRO, "Ethanol steam reforming over Ni/MxOyNi/MxOy–Al2O3Al2O3 (M=CeM=Ce, La, Zr and Mg) catalysts: Influence of support on the hydrogen production," *Int. J. Hydrogen Energy*, vol. 32, no. 10–11, pp. 1462–1471, Jul. 2007, doi: 10.1016/j.ijhydene.2006.10.025.

[8] J. Sun, A. Gao, X. Wang, X. Xu, and J. Song, "Removal of Phosphorus from Wastewater by Different Morphological Alumina," *Molecules*, vol. 25, no. 13, p. 3092, Jul. 2020, doi: 10.3390/molecules25133092.

[9] W. Gac, W. Zawadzki, M. Rotko, M. Greluk, G. Słowik, and G. Kolb, "Effects of support composition on the performance of nickel catalysts in CO2 methanation reaction," *Catal.*

Today, vol. 357, pp. 468–482, Nov. 2020, doi: 10.1016/j.cattod.2019.07.026.

[10] F. Yang *et al.*, "Size Dependence of Vapor Phase Hydrodeoxygenation of m -Cresol on Ni/SiO 2 Catalysts," *ACS Catal.*, vol. 8, no. 3, pp. 1672–1682, Mar. 2018, doi: 10.1021/acscatal.7b04097.

[11] O. J. Olusola and M. Sudip, "Temperature programme reduction (TPR) studies of cobalt phases in -alumina supported cobalt catalysts," *J. Pet. Technol. Altern. Fuels*, vol. 7, no. 1, pp. 1–12, Jan. 2016, doi: 10.5897/JPTAF2015.0122.

[12] J. Li, G. Lu, G. Wu, D. Mao, Y. Wang, and Y. Guo, "Promotional role of ceria on cobaltosic oxide catalyst for low-temperature CO oxidation," *Catal. Sci. Technol.*, vol. 2, no. 9, p. 1865, 2012, doi: 10.1039/c2cy20118f.

[13] R. Munirathinam, D. Pham Minh, and A. Nzihou, "Effect of the Support and Its Surface Modifications in Cobalt-Based Fischer–Tropsch Synthesis," *Ind. Eng. Chem. Res.*, vol. 57, no. 48, pp. 16137–16161, Dec. 2018, doi: 10.1021/acs.iecr.8b03850.

[14] H. Xiong, Y. Zhang, K. Liew, and J. Li, "Catalytic performance of zirconium-modified Co/Al2O3 for Fischer–Tropsch synthesis," *J. Mol. Catal. A Chem.*, vol. 231, no. 1–2, pp. 145–151, Apr. 2005, doi: 10.1016/j.molcata.2004.12.033.

[15] E. S. Lokteva and E. V. Golubina, "Metal-support interactions in the design of heterogeneous catalysts for redox processes," *Pure Appl. Chem.*, vol. 91, no. 4, pp. 609–631, Apr. 2019, doi: 10.1515/pac-2018-0715.

[16] A. G. Sato, D. P. Volanti, D. M. Meira, S. Damyanova, E. Longo, and J. M. C. Bueno, "Effect of the ZrO2 phase on the structure and behavior of supported Cu catalysts for ethanol conversion," *J. Catal.*, vol. 307, pp. 1–17, Nov. 2013, doi: 10.1016/j.jcat.2013.06.022.

[17] F. K. McTAGGART, "Reduction of Zirconium and Hafnium Oxides," *Nature*, vol. 191, no. 4794, pp. 1192–1192, Sep. 1961, doi: 10.1038/1911192a0.

[18] D.-L. Hoang, H. Berndt, and H. Lieske, "Hydrogen spillover phenomena on Pt/ZrO2," *Catal. Letters*, vol. 31, no. 2–3, pp. 165–172, Jun. 1995, doi: 10.1007/BF00808830.

[19] K.-D. Jung and A. T. Bell, “Role of Hydrogen Spillover in Methanol Synthesis over Cu/ZrO2,” *J. Catal.*, vol. 193, no. 2, pp. 207–223, Jul. 2000, doi: 10.1006/jcat.2000.2881.

[20] Y. Zheng, N. Zhao, and J. Chen, “Enhanced direct deoxygenation of anisole to benzene on SiO2-supported Ni-Ga alloy and intermetallic compound,” *Appl. Catal. B Environ.*, vol. 250, pp. 280–291, Aug. 2019, doi: 10.1016/j.apcatb.2019.02.073.

[21] N. Mironova-Ulmane, A. Kuzmin, I. Sildos, L. Puust, and J. Grabis, “Magnon and Phonon Excitations in Nanosized NiO,” *Latv. J. Phys. Tech. Sci.*, vol. 56, no. 2, pp. 61–72, Apr. 2019, doi: 10.2478/lpts-2019-0014.

[22] E. Meza Fuentes, J. I. Rodriguez Ruiz, and M. do C. Rangel Santos, “Characteristics of NiO present in solids obtained from hydrotalcites based on Ni/Al and Ni-Zn/Al,” *DYNA*, vol. 86, no. 210, pp. 58–65, Jul. 2019, doi: 10.15446/dyna.v86n210.78559.

[23] M. Rashad, M. Rüsing, G. Berth, K. Lischka, and A. Pawlis, “CuO and Co 3 O 4 Nanoparticles: Synthesis, Characterizations, and Raman Spectroscopy,” *J. Nanomater.*, vol. 2013, pp. 1–6, 2013, doi: 10.1155/2013/714853.

[24] V. G. Hadjiev, M. N. Iliev, and I. V Vergilov, “The Raman spectra of Co3O4,” *J. Phys. C Solid State Phys.*, vol. 21, no. 7, pp. L199–L201, Mar. 1988, doi: 10.1088/0022-3719/21/7/007.

[25] A. P. Naumenko, N. Berezovska, M. M. Biliy, and O. V Shevchenko, “Vibrational analysis and Raman spectra of tetragonal zirconia,” *Phys. Chem. Solid state*, vol. 9, no. 1, pp. 121–125, 2008, [Online]. Available: https://www.researchgate.net/publication/285329926.

[26] I. E. Wachs, F. D. Hardcastle, and S. S. Chan, “Raman spectroscopy of supported metal oxide catalysts,” *Spectroscopy*, vol. 1, no. 8, pp. 30–38, 1986.

[27] A. Primo *et al.*, “High catalytic activity of oriented 2.0.0 copper(I) oxide grown on graphene film,” *Nat. Commun.*, vol. 6, no. 1, p. 8561, Dec. 2015, doi: 10.1038/ncomms9561.